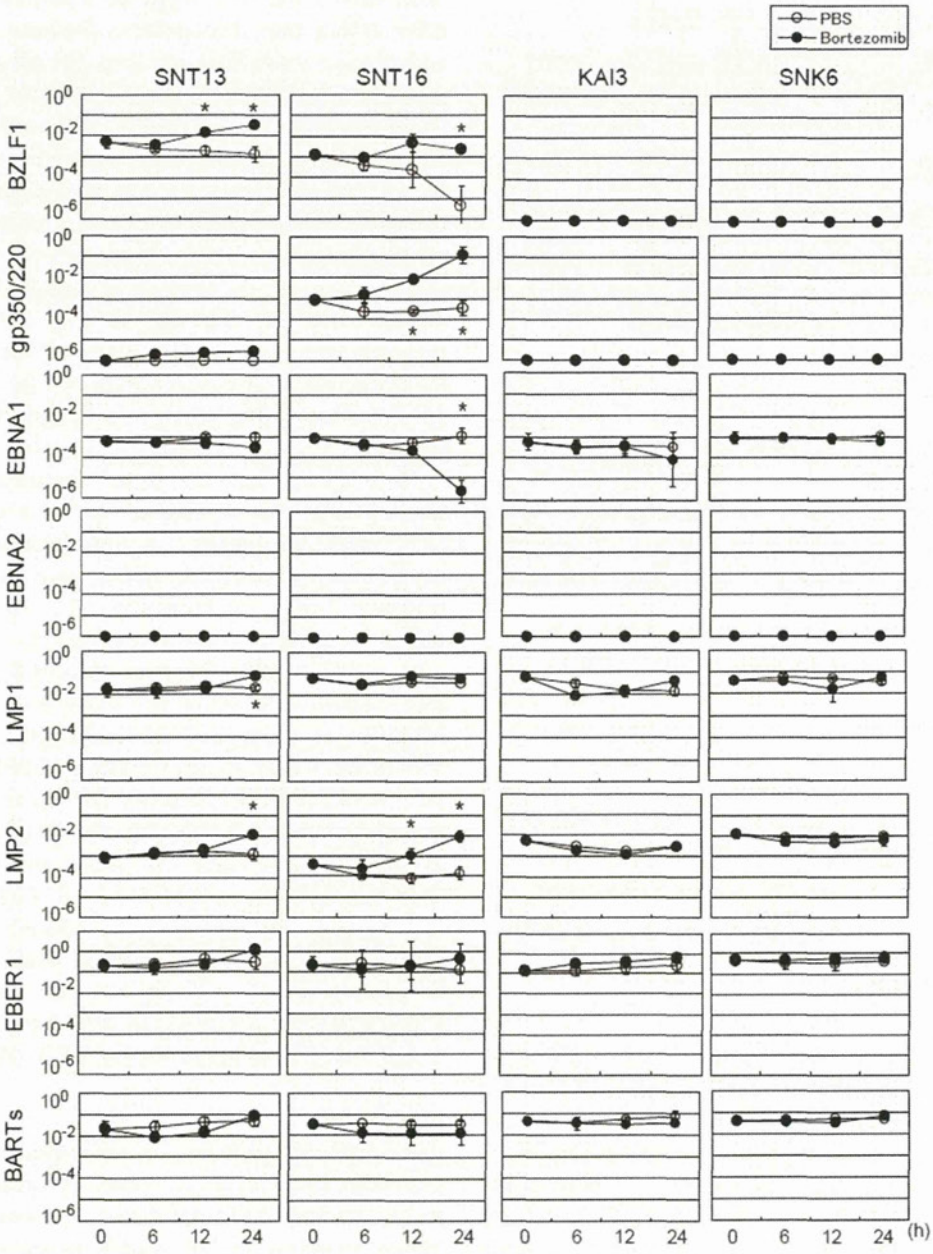

Figure 5. Bortezomib induces lytic infection of EBV in T cell lines. EBV-positive T cell lines (SNT-13 and SNT-16) and EBV-positive NK cell lines (KAI-3 and SNK-6) were treated with 1 μM bortezomib and collected at 0, 6, 12, and 24 hr to evaluate the expression of EBV-encoded genes by real-time RT-PCR. BZLF1 is an immediate early gene and gp350/220 is a late gene. EBNA1, EBNA2, LMP1, LMP2, EBER1, and BARTs are latent genes. β2-microglobulin was used as an endogenous control and reference gene for relative quantification and assigned an arbitrary value of 1 (10^0). Closed circles indicate bortezomib-treated cells, while open circles denote PBS-treated cells. Bars indicate standard errors. *$p < 0.05$ by Mann-Whitney *U*-test.

that this apoptosis was due to bortezomib inhibiting the degradation of phosphorylated IκB.[8,14,36] The inhibition of phosphorylated IκB degradation restrains the activation of NF-κB, which is associated with chemoresistance and poor survival in T and NK cell lymphomas.[37,38] We found, however, no significant difference between EBV-positive and -negative cell lines. The findings suggest that the mechanism of bortezomib in eliminating malignant cells involves the inhibition of NF-κB activation inducing apoptosis and preventing the immortalization and proliferation of cells. Other mechanisms by which bortezomib acts against malignancies, such as the stabilization of p53, disruption of the cell cycle, induction of endoplasmic reticulum stress, and increased intracellular reactive oxygen species, have been reported.[39,40]

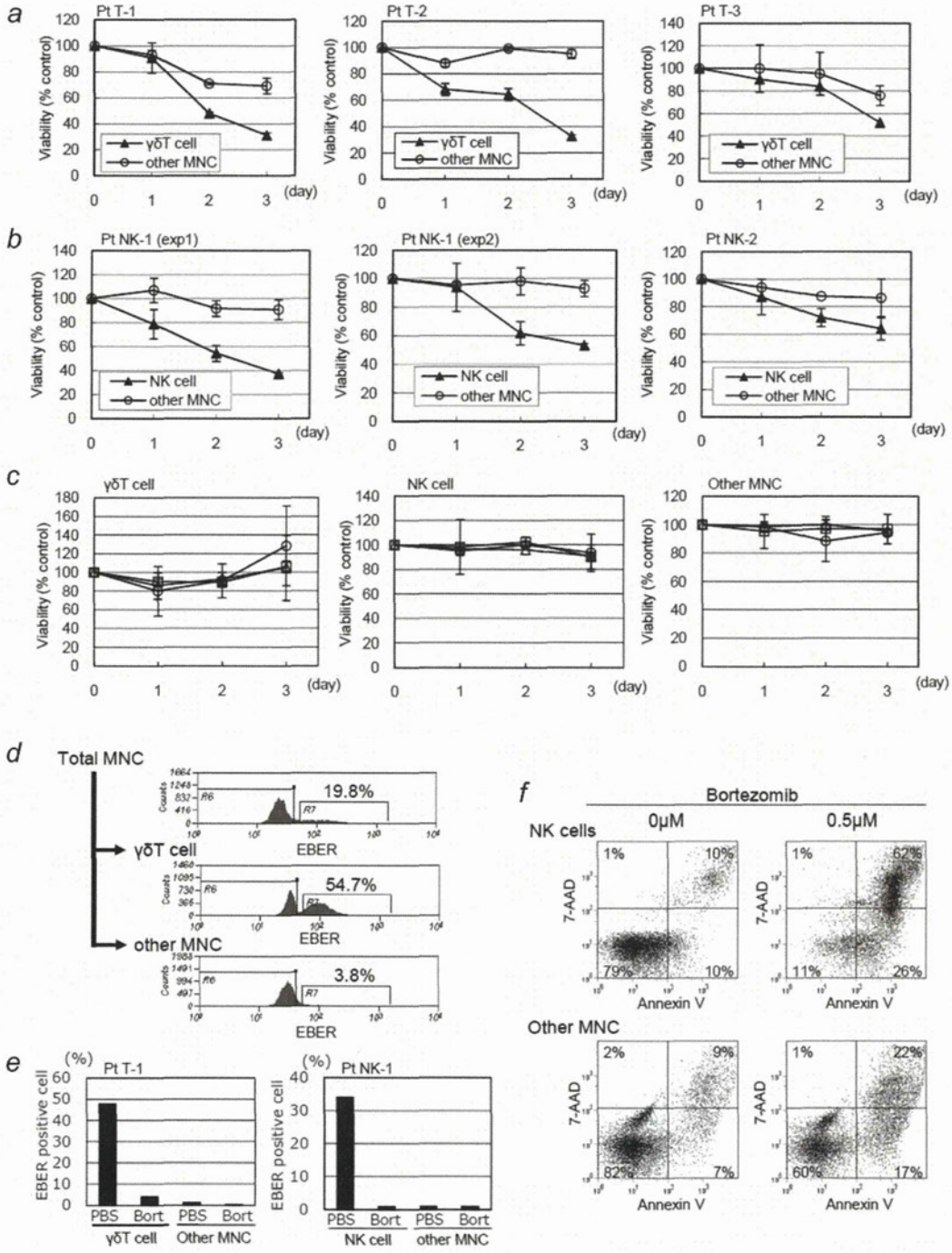

Figure 6. Bortezomib decreases the viability of EBV-infected cells from patients with EBV-associated diseases. (*a, b, c*) Bortezomib (0.5 μM) was administered to each sample of cells, and the viable cells were counted for 3 days. (*a*) γδT cells and other MNCs from three patients (Patients T-1, T-2, and T-3) with hydroa vacciniforme-like lymphoma, (*b*) NK cells and other MNCs from two patients (Patients NK-1, and NK-2) with NK cell-type chronic active EBV infection, and (*c*) γδT cell, NK cell, and non-γδT, non-NK cell (other MNC) from three healthy donors were separated by magnetic sorting. For Patient NK-1, experiments were performed twice on different visits (exp.1 and exp.2). Bars indicate standard errors. (*d*) EBER-positive cells of Patient T-1 with hydroa vacciniforme-like lymphoma were quantified using a FISH assay on unsorted MNCs (total MNCs), the γδT cell fraction (γδT cell), and the non-γδT cell fraction (other MNCs). (*e*) The EBER-positive rate of each sorted cells from Patient T-1 (left) and Patient NK-1 (right) were quantified using a FISH assay after 3 days treatment with bortezomib or PBS. (*f*) NK cells and other MNCs of Patient NK-1, with NK cell-type chronic active EBV infection were separated by magnetic sorting. Cells were treated with 0.5 μM bortezomib for 24 hr and analyzed by flow cytometry. Viable cells were defined as those negative for annexin V-PE and 7-AAD staining, and early apoptotic cells were defined as those positive for annexin V-PE and negative for 7-AAD staining.

The existence of EBV may have little effect on cell death induced by bortezomib. In a previous study, the killing effect of bortezomib was not different between EBV-positive and -negative Burkitt lymphoma cell lines,[8,41] although Zou *et al.*[8] reported that bortezomib had a greater effect in B cell lines with latency type III than those with Type I. The effect of bortezomib may be different in cells with different latency types due to distinct patterns of viral gene expression. The existence of EBV may have some effect on bortezomib because LMP1 is known to activate NF-κB.[42] In the study by Zou *et al.*,[8] however, transfection of LMP1 into an EBV-negative B cell line did not change the sensitivity to bortezomib. The EBV-positive T and NK cell lines used in our study are classified as latency type II[25] and express LMP1. Bortezomib seemed to have little impact on LMP1-mediated NF-κB activation because the presence of EBV did not influence its effects in our study. Comparing cell lines that are naturally EBV positive with derivative cell lines that have lost EBV is necessary to prove that EBV does not affect the outcome of bortezomib treatment. However, establishing such EBV-depleted cell lines is very difficult and, to our knowledge, there are no existing EBV-depleted T- or NK-cell lines. Alternatively, we compared EBV-negative cell lines and those that have been infected with EBV *in vitro*. We admit that this is an artificial system that may have limited relevance.

Bortezomib induced lytic infection only in T cell lines. Inhibition of the NF-κB pathway has been shown to induce the EBV lytic cycle.[43] Although the reason for the difference in lytic induction between T and NK cell lines is unclear, T cell lines seem to express lytic infection genes more often than NK cell lines, consistent with our previous report.[25] Histone deacetylase inhibitors, such as butyric acid and valproic acid, and phorbol 12-myristate 13-acetate are reported to induce an EBV lytic cycle in B cell and epithelial cell lines.[5,26] To our knowledge, however, no agent induces a lytic cycle in EBV-positive NK cell lines. We administered valproic acid, a class I histone deacetylase inhibitor, to NK-cell lymphoma cell lines. Lytic induction was not induced in the NK cell lines (data not shown).

Such lytic induction could contribute to the decreased viability of T cell lines. However, this lytic induction is not a major mechanism of bortezomib-induced cell death because no significant difference was observed in its effect between T and NK cell lines, or between EBV-positive and -negative cell lines. In SNT-16 cells, bortezomib induced a marked decrease in viability, and the recovery in viability following administration of a pan-caspase inhibitor was incomplete (Fig. 3*c*). Thus, the induction of lytic infection by bortezomib could play a partial role in this cell line. Additionally, this result suggests the potential utility of bortezomib as a novel strategy against EBV-positive T cell lymphoma. In EBV-infected T cells, a few latent genes with low antigenicity are expressed.[25] Moreover, the increased expression of lytic proteins, which are generally antigenic, can be recognized in virus-specific cytotoxic T lymphocytes, resulting in lysis of EBV-infected T cells.

Bortezomib killed EBV-infected γδT cells of hydroa vacciniforme-like lymphoma and EBV-infected NK cells of chronic active EBV infection. Taken together with the flow cytometry results, bortezomib induced apoptosis in EBV-infected immortalized cells. These results indicate that bortezomib may be an effective therapy against EBV-associated T and NK lymphoma/lymphoproliferative diseases. We administered 0.5 μM bortezomib to peripheral blood cells in an *ex vivo* study. This concentration is approximately equal to the plasma concentration after administering 1.3 mg/m^2 bortezomib in a recent Phase I and II study of multiple myeloma.[44]

Although recent studies have shown that the effect of bortezomib could be enhanced synergistically in combination with a histone deacetylase inhibitor,[45–47] further studies with appropriate *in vivo* models are essential to confirm this possibility. EBV infects only humans and no good animal models exist, although recently, humanized mouse models with reconstituted human lymphocytes and EBV infection have been reported.[48–50] Despite the complexity of this mouse model, it could be useful for evaluating new therapies, including molecular targeted therapy. The *ex vivo* administration model, coupled with magnetic sorting, is a convenient method to evaluate molecular targeted therapy against EBV-associated lymphoma.

In conclusion, bortezomib killed T/NK lymphoma cells by inducing apoptosis. No significant difference in killing was observed between EBV-positive and -negative cell lines, although bortezomib induced lytic infection in EBV-infected T cells. Following *ex vivo* administration, bortezomib had a greater killing effect on EBV-positive cells than other MNCs. These results give rationale for the use of bortezomib on T/NK lymphomas, although existence of EBV may have little effect on cell death induced by bortezomib.

Acknowledgements

We thank Norio Shimizu (Tokyo Medical and Dental University) and Ayako Demachi-Okamura (Aichi Cancer Center) for the SNK-6, SNT-13 and SNT-16 cell lines. KAI3 and KHYG-1 were obtained from the Japanese Collection of Research Bioresources. We also thank Millennium Pharmaceuticals Inc. for providing the bortezomib.
All authors have no conflict.

References

1. Cohen JI. Epstein-Barr virus infection. *N Engl J Med* 2000;343:481–92.
2. Quintanilla-Martinez L, Kumar H, Jaffe ES. EBV$^+$ T-cell lymphoma of childhood. In: Jaffe ES, Harris NL, Stein H, eds. WHO classification of tumours of haematopoietic and lymphoid tissues, 4th edn. Lyon: IARC Press, 2008278–28.
3. Rickinson AB, Kieff E. Epstein-Barr virus. In: Knipe DM, Howley PM, eds. Fields virology, vol. 2. Philadelphia, PA: Lippincott Williams & Wilkins, 20072655–700.
4. Williams H, Crawford DH. Epstein-Barr virus: the impact of scientific advances on clinical practice. *Blood* 2006;107:862–9.

5. Kieff ED, Rickinson AV. Epstein-Barr virus and its replication. In: Knipe DM, Howley PM, eds. Fields virology, vol.2. Philadelphia. PA: Lippincott Williams & Wilkins, 2007.2603–54.
6. Cartron G, Watier H, Golay J, Solal-Celigny P. From the bench to the bedside: ways to improve rituximab efficacy. *Blood* 2004;104:2635–42.
7. Heslop HE. How I treat EBV lymphoproliferation. *Blood* 2009;114: 4002–8.
8. Zou P, Kawada J, Pesnicak L, Cohen JI. Bortezomib induces apoptosis of Epstein-Barr virus (EBV)-transformed B cells and prolongs survival of mice inoculated with EBV-transformed B cells. *J Virol* 2007;81: 10029–36.
9. Adams J. Proteasome inhibition: a novel approach to cancer therapy. *Trends Mol Med* 2002;8:S49–54.
10. Orlowski RZ, Eswara JR, Lafond-Walker A, Grever MR, Orlowski M, Dang CV. Tumor growth inhibition induced in a murine model of human Burkitt's lymphoma by a proteasome inhibitor. *Cancer Res* 1998;58: 4342–8.
11. Zhang XM, Lin H, Chen C, Chen BD. Inhibition of ubiquitin-proteasome pathway activates a caspase-3-like protease and induces Bcl-2 cleavage in human M-07e leukaemic cells. *Biochem J* 1999;340(Pt 1):127–33.
12. Jackson G, Einsele H, Moreau P, Miguel JS. Bortezomib, a novel proteasome inhibitor, in the treatment of hematologic malignancies. *Cancer Treat Rev* 2005;31: 591–602.
13. Richardson PG, Mitsiades C, Hideshima T, Anderson KC. Bortezomib: proteasome inhibition as an effective anticancer therapy. *Annu Rev Med* 2006;57:33–47.
14. Paramore A, Frantz S. Bortezomib. *Nat Rev Drug Discov* 2003;2:611–2.
15. Fu DX, Tanhehco YC, Chen J, Foss CA, Fox JJ, Lemas V, Chong JM, Ambinder RF, Pomper MG. Virus-associated tumor imaging by induction of viral gene expression. *Clin Cancer Res* 2007;13:1453–8.
16. Pulvertaft JV. A study of malignant tumours in Nigeria by short-term tissue culture. *J Clin Pathol* 1965;18:261–73.
17. Zhang Y, Nagata H, Ikeuchi T, Mukai H, Oyoshi MK, Demachi A, Morio T, Wakiguchi H, Kimura N, Shimizu N, Yamamoto K. Common cytological and cytogenetic features of Epstein-Barr virus (EBV)-positive natural killer (NK) cells and cell lines derived from patients with nasal T/NK-cell lymphomas, chronic active EBV infection and hydroa vacciniforme-like eruptions. *Br J Haematol* 2003;121:805–14.
18. Tsuge I, Morishima T, Morita M, Kimura H, Kuzushima K, Matsuoka H. Characterization of Epstein-Barr virus (EBV)-infected natural killer (NK) cell proliferation in patients with severe mosquito allergy; establishment of an IL-2-dependent NK-like cell line. *Clin Exp Immunol* 1999;115:385–92.
19. Kaplan J, Tilton J, Peterson WD, Jr. Identification of T cell lymphoma tumor antigens on human T cell lines. *Am J Hematol* 1976;1:219–23.
20. Yagita M, Huang CL, Umehara H, Matsuo Y, Tabata R, Miyake M, Konaka Y, Takatsuki K. A novel natural killer cell line (KHYG-1) from a patient with aggressive natural killer cell leukemia carrying a p53 point mutation. *Leukemia* 2000;14:922–30.
21. Miyoshi I, Kubonishi I, Yoshimoto S, Akagi T, Ohtsuki Y, Shiraishi Y, Nagata K, Hinuma Y. Type C virus particles in a cord T-cell line derived by co-cultivating normal human cord leukocytes and human leukaemic T cells. *Nature* 1981;294:770–1.
22. Fujiwara S, Ono Y. Isolation of Epstein-Barr virus-infected clones of the human T-cell line MT-2: use of recombinant viruses with a positive selection marker. *J Virol* 1995;69:3900–3.
23. Robertson MJ, Cochran KJ, Cameron C, Le JM, Tantravahi R, Ritz J. Characterization of a cell line, NKL, derived from an aggressive human natural killer cell leukemia. *Exp Hematol* 1996;24:406–15.
24. Isobe Y, Sugimoto K, Matsuura I, Takada K, Oshimi K. Epstein-Barr virus renders the infected natural killer cell line, NKL resistant to doxorubicin-induced apoptosis. *Br J Cancer* 2008;99:1816–22.
25. Iwata S, Wada K, Tobita S, Gotoh K, Ito Y, Demachi-Okamura A, Shimizu N, Nishiyama Y, Kimura H. Quantitative analysis of Epstein-Barr virus (EBV)-related gene expression in patients with chronic active EBV infection. *J Gen Virol* 2010;91:42–50.
26. Kubota N, Wada K, Ito Y, Shimoyama Y, Nakamura S, Nishiyama Y, Kimura H. One-step multiplex real-time PCR assay to analyse the latency patterns of Epstein-Barr virus infection. *J Virol Methods* 2008;147: 26–36.
27. Patel K, Whelan PJ, Prescott S, Brownhill SC, Johnston CF, Selby PJ, Burchill SA. The use of real-time reverse transcription-PCR for prostate-specific antigen mRNA to discriminate between blood samples from healthy volunteers and from patients with metastatic prostate cancer. *Clin Cancer Res* 2004;10:7511–9.
28. Kimura H, Miyake K, Yamauchi Y, Nishiyama K, Iwata S, Iwatsuki K, Gotoh K, Kojima S, Ito Y, Nishiyama Y. Identification of Epstein-Barr virus (EBV)-infected lymphocyte subtypes by flow cytometric in situ hybridization in EBV-associated lymphoproliferative diseases. *J Infect Dis* 2009;200:1078–87.
29. Kimura H, Hoshino Y, Hara S, Sugaya N, Kawada J, Shibata Y, Kojima S, Nagasaka T, Kuzushima K, Morishima T. Differences between T cell-type and natural killer cell-type chronic active Epstein-Barr virus infection. *J Infect Dis* 2005;191:531–9.
30. Kimura H, Hoshino Y, Kanegane H, Tsuge I, Okamura T, Kawa K, Morishima T. Clinical and virologic characteristics of chronic active Epstein-Barr virus infection. *Blood* 2001;98:280–6.
31. Kimura H, Morishima T, Kanegane H, Ohga S, Hoshino Y, Maeda A, Imai S, Okano M, Morio T, Yokota S, Tsuchiya S, Yachie A, et al. Prognostic factors for chronic active Epstein-Barr virus infection. *J Infect Dis* 2003;187:527–33.
32. Shen L, Au WY, Guo T, Wong KY, Wong ML, Tsuchiyama J, Yuen PW, Kwong YL, Liang RH, Srivastava G. Proteasome inhibitor bortezomib-induced apoptosis in natural killer (NK)-cell leukemia and lymphoma: an in vitro and in vivo preclinical evaluation. *Blood* 2007;110: 469–70.
33. Shen L, Au WY, Wong KY, Shimizu N, Tsuchiyama J, Kwong YL, Liang RH, Srivastava G. Cell death by bortezomib-induced mitotic catastrophe in natural killer lymphoma cells. *Mol Cancer Ther* 2008;7:3807–15.
34. Lee J, Suh C, Kang HJ, Ryoo BY, Huh J, Ko YH, Eom HS, Kim K, Park K, Kim WS. Phase I study of proteasome inhibitor bortezomib plus CHOP in patients with advanced, aggressive T-cell or NK/T-cell lymphoma. *Ann Oncol* 2008;19:2079–83.
35. Zinzani PL, Musuraca G, Tani M, Stefoni V, Marchi E, Fina M, Pellegrini C, Alinari L, Derenzini E, de Vivo A, Sabattini E, Pileri S, et al. Phase II trial of proteasome inhibitor bortezomib in patients with relapsed or refractory cutaneous T-cell lymphoma. *J Clin Oncol* 2007;25:4293–7.
36. Hideshima T, Richardson P, Chauhan D, Palombella VJ, Elliott PJ, Adams J, Anderson KC. The proteasome inhibitor PS-341 inhibits growth, induces apoptosis, and overcomes drug resistance in human multiple myeloma cells. *Cancer Res* 2001; 61:3071–6.
37. Kim K, Ryu K, Ko Y, Park C. Effects of nuclear factor-kappaB inhibitors and its implication on natural killer T-cell lymphoma cells. *Br J Haematol* 2005;131: 59–66.
38. Liu X, Wang B, Ma X, Guo Y. NF-kappaB activation through the alternative pathway correlates with chemoresistance and poor survival in extranodal NK/T-cell lymphoma, nasal type. *Jpn J Clin Oncol* 2009;39:418–24.
39. Chen S, Blank JL, Peters T, Liu XJ, Rappoli DM, Pickard MD, Menon S, Yu J, Driscoll DL, Lingaraj T, Burkhardt AL, Chen W,

et al. Genome-wide siRNA screen for modulators of cell death induced by proteasome inhibitor bortezomib. *Cancer Res* 2010;70:4318–26.
40. Nencioni A, Grunebach F, Patrone F, Ballestrero A, Brossart P. Proteasome inhibitors: antitumor effects and beyond. *Leukemia* 2007;21:30–6.
41. Cordova C, Munker R. The presence or absence of latent Epstein-Barr virus does not alter the sensitivity of Burkitt's lymphoma cell lines to proteasome inhibitors. *Acta Haematol* 2008;119:241–3.
42. Shair KH, Bendt KM, Edwards RH, Bedford EC, Nielsen JN, Raab-Traub N. EBV latent membrane protein 1 activates Akt, NFkappaB, and Stat3 in B cell lymphomas. *PLoS Pathog* 2007;3:e166.
43. Brown HJ, Song MJ, Deng H, Wu TT, Cheng G, Sun R. NF-kappaB inhibits gammaherpesvirus lytic replication. *J Virol* 2003;77:8532–40.
44. Ogawa Y, Tobinai K, Ogura M, Ando K, Tsuchiya T, Kobayashi Y, Watanabe T, Maruyama D, Morishima Y, Kagami Y, Taji H, Minami H, et al. Phase I and II pharmacokinetic and pharmacodynamic study of the proteasome inhibitor bortezomib in Japanese patients with relapsed or refractory multiple myeloma. *Cancer Sci* 2008;99:140–4.
45. Heider U, Rademacher J, Lamottke B, Mieth M, Moebs M, von Metzler I, Assaf C, Sezer O. Synergistic interaction of the histone deacetylase inhibitor SAHA with the proteasome inhibitor bortezomib in cutaneous T cell lymphoma. *Eur J Haematol* 2009;82:440–9.
46. Kawada J, Zou P, Mazitschek R, Bradner JE, Cohen JI. Tubacin kills Epstein-Barr virus (EBV)-Burkitt lymphoma cells by inducing reactive oxygen species and EBV lymphoblastoid cells by inducing apoptosis. *J Biol Chem* 2009;284:17102–9.
47. Stamatopoulos B, Meuleman N, De Bruyn C, Mineur P, Martiat P, Bron D, Lagneaux L. Antileukemic activity of valproic acid in chronic lymphocytic leukemia B cells defined by microarray analysis. *Leukemia* 2009;23:2281–9.
48. Yajima M, Imadome K, Nakagawa A, Watanabe S, Terashima K, Nakamura H, Ito M, Shimizu N, Honda M, Yamamoto N, Fujiwara S. A new humanized mouse model of Epstein-Barr virus infection that reproduces persistent infection, lymphoproliferative disorder, and cell-mediated and humoral immune responses. *J Infect Dis* 2008;198:673–82.
49. Hong GK, Gulley ML, Feng WH, Delecluse HJ, Holley-Guthrie E, Kenney SC. Epstein-Barr virus lytic infection contributes to lymphoproliferative disease in a SCID mouse model. *J Virol* 2005;79:13993–4003.
50. Strowig T, Gurer C, Ploss A, Liu YF, Arrey F, Sashihara J, Koo G, Rice CM, Young JW, Chadburn A, Cohen JI, Munz C. Priming of protective T cell responses against virus-induced tumors in mice with human immune system components. *J Exp Med* 2009;206:1423–34.

OPEN ACCESS Freely available online

PLoS one

Replication of Epstein-Barr Virus Primary Infection in Human Tonsil Tissue Explants

Kensei Gotoh[1], Yoshinori Ito[1]*, Seiji Maruo[2], Kenzo Takada[2], Terukazu Mizuno[3], Masaaki Teranishi[3], Seiichi Nakata[3], Tsutomu Nakashima[3], Seiko Iwata[4], Fumi Goshima[4], Shigeo Nakamura[5], Hiroshi Kimura[4]

1 Department of Pediatrics, Nagoya University Graduate School of Medicine, Nagoya, Japan, **2** Department of Tumor Virology, Institute for Genetic Medicine, Hokkaido University, Sapporo, Japan, **3** Department of Otorhinolaryngology, Nagoya University Graduate School of Medicine, Nagoya, Japan, **4** Department of Virology, Nagoya University Graduate School of Medicine, Nagoya, Japan, **5** Department of Pathology and Laboratory Medicine, Nagoya University Hospital, Nagoya, Japan

Abstract

Epstein-Barr virus (EBV) may cause a variety of virus-associated diseases, but no antiviral agents have yet been developed against this virus. Animal models are thus indispensable for the pathological analysis of EBV-related infections and the elucidation of therapeutic methods. To establish a model system for the study of EBV infection, we tested the ability of B95–8 virus and recombinant EBV expressing enhanced green fluorescent protein (EGFP) to replicate in human lymphoid tissue. Human tonsil tissues that had been surgically removed during routine tonsillectomy were sectioned into small blocks and placed on top of collagen sponge gels in culture medium at the air-interface, then a cell-free viral suspension was directly applied to the top of each tissue block. Increasing levels of EBV DNA in culture medium were observed after 12–15 days through 24 days post-infection in tissue models infected with B95–8 and EGFP-EBV. Expression levels of eight EBV-associated genes in cells collected from culture medium were increased during culture. EBV-encoded small RNA-positive cells were detected in the interfollicular areas in paraffin-embedded sections. Flow cytometric analyses revealed that most $EGFP^+$ cells were $CD3^-$ $CD56^-$ $CD19^+$ HLA-DR^+, and represented both naïve (immunoglobulin D^+) and memory ($CD27^+$) B cells. Moreover, EBV replication in this model was suppressed by acyclovir treatment in a dose-dependent manner. These data suggest that this model has potential for use in the pathological analysis of local tissues at the time of primary infection, as well as for screening novel antiviral agents.

Citation: Gotoh K, Ito Y, Maruo S, Takada K, Mizuno T, et al. (2011) Replication of Epstein-Barr Virus Primary Infection in Human Tonsil Tissue Explants. PLoS ONE 6(10): e25490. doi:10.1371/journal.pone.0025490

Editor: Luwen Zhang, University of Nebraska – Lincoln, United States of America

Received February 25, 2011; **Accepted** September 6, 2011; **Published** October 5, 2011

Funding: This study was supported by grants from the Japan Society for the Promotion of Science (20591276) to YI and from Health and Labour Science Research (22091401) to YI and HK. The funders had no role in study design, data collection and analysis, decision to publish, or preparation of the manuscript.

Competing Interests: The authors have declared that no competing interests exist.

* E-mail: yoshi-i@med.nagoya-u.ac.jp

Introduction

Epstein-Barr Virus (EBV) is a universal human γ-herpesvirus, generally transmitted via saliva, with the oropharynx as the site of infection [1,2]. Primary EBV infection occurs most frequently in infancy and childhood, and in many cases causes either no or only nonspecific symptoms. In cases of primary infection among adolescents and young adults, infectious mononucleosis (IM) often develops, and the course may sometimes be severe or fatal. After infection, EBV remains in most adults as an asymptomatic latent infection, but may cause neoplastic disorders such as Burkitt's lymphoma or post-transplant lymphoproliferative disorder (PTLD).

Although EBV may cause a variety of disorders, no vaccine or antiviral agent has yet been developed against this virus [1,2]. In general, animal models are indispensable for the pathological analysis of viral infections and the elucidation of methods of treatment and prevention, but EBV only infects humans in nature and limited animal species under experimental conditions. Various infection models have been used to investigate EBV-associated diseases [3,4,5,6,7]. Mouse models that partially reconstitute human immune system components after engagement of hematopoietic progenitor cells are of particular interest, because they reproduce human immunity and diseases caused by EBV. Several mouse models of immunodeficiency have been applied, including $Rag2^{-/-}$ $\gamma c^{-/-}$ mice [8,9], NOD/SCID mice [10], NOD/SCID/$\gamma c^{-/-}$ mice [11,12,13], BLT mice (NOD/SCID mice with implantation of human fetal liver and thymus pieces under the renal capsule) [14], and NOD/Shi-SCID/IL-2Rγ^{null} (NOG) mice [15]. Of these, the NOG mice model [15] has been used to show that B-cell lymphoproliferative disorder arises during EBV infection with a high viral load, whereas asymptomatic persistent infection arises from infection with a low viral load. In addition, EBV-specific T-cell responses and EBV-specific antibodies were detected in blood, revealing this mouse model as a useful tool for investigating the pathogenesis, prevention, and treatment of EBV infection. Culture models using human lymphatic tissues, however, appear advantageous for the study of localized pathology in EBV infection. We therefore focused on a model of infection using human tonsillar lymphoid tissues.

Numerous reports have described the use of viral infection models using human tonsillar lymphoid tissues for the study of human immunodeficiency virus (HIV) [16], while others have described the use of such models for investigating other members

of the herpesvirus family, such as human herpesvirus (HHV)-6, HHV-7, and herpes simplex virus (HSV)-2 [17,18,19]. The palatine tonsils comprise typical lymphoid tissue and are also the natural portal of entry for EBV, thus showing great potential for reproducing the pathology of primary infection with EBV. The present study used human tonsillar lymphoid tissues to establish an EBV infection model and investigated infected cells during the initial stage of infection. We also tested the utility of this model as a screening system for antiviral agents.

Materials and Methods

Ethics statement

Human subject protocols were approved by the institutional review board of Nagoya University School of Medicine (2006-450). Written informed consent was provided by study participants and/or their legal guardians prior to enrolment.

Virus stocks

Cell-free virus solution was obtained from culture supernatant of B95–8 cells (an EBV-infected marmoset cell line) (ATCC) after centrifuging for 5 min at 3,000×*g* and filtration through a 0.45-μm membrane filter. In some experiments, we also used supernatants containing recombinant EBV expressing enhanced green fluorescent protein (EGFP), in which a gene cassette consisting of the EGFP gene driven by the simian virus 40 promoter and a neomycin resistance gene driven by the simian virus 40 promoter were inserted into the viral BXLF1 gene [20]. Titers of virus in the 50% transforming dose (TD_{50}) were determined using the Reed-Muench method, as described elsewhere [15,21]. Calculated titers were 1×10^2 TD_{50}/ml for B95 and 1×10^3 TD_{50}/ml for EGFP-EBV.

Tissue culture and viral infection

Human tonsils surgically removed during routine tonsillectomy and not required for clinical purposes were received within several hours of excision, then dissected, cultured, and infected, as described elsewhere [16,22,23]. Since EBV-specific immune responses may impact cellular infection, we only used tonsils from EBV-seronegative individuals. Serological tests for anti-EBV antibodies were examined 2–4 weeks preoperatively and negative results for viral capsid antigen immunoglobulin (Ig) G and EBV nuclear antigen were confirmed. In brief, the tonsils were washed thoroughly with medium containing antibiotics, sectioned into cubes with an average weight of 5 mg, and placed on top of collagen sponge gels in culture medium at the air-interface. For EBV infection, 10 μL of clarified viral suspension was directly applied on top of each tissue block. The culture medium used to bathe 54 tissue blocks in six wells was collected every 3 days after viral inoculation. Cell-free supernatants and cells were obtained after centrifugation of collected medium and used for the following assays. Cells collected from culture medium were considered to have come from infected tissues. Most of the epithelial tonsillar layers were lost during preparation of tissue blocks, so replication of EBV in epithelial cells could not be examined.

Quantification of EBV DNA

Viral DNA was extracted from either 200 μL of cell-free culture supernatants or from 5×10^5 cells collected from culture medium using QIAamp DNA blood kits (Qiagen). Real-time quantitative PCR assays were performed as previously described [24,25,26].

RNA purification and real-time RT-PCR

RNA was extracted from 5×10^5 cells from culture medium with a QIAmp RNeasy Mini Kit (Qiagen). Viral mRNA expression was quantified by one-step multiplex real-time reverse transcription (RT)-PCR using the Mx3000P real-time PCR system (Stratagene), as described previously [27,28], to examine expression levels of two lytic genes (BZLF1 and gp350/220) and six latent genes (EBV-encoded nuclear antigen (EBNA)1, EBNA2, latent membrane protein (LMP)1, LMP2, EBV-encoded small RNA (EBER)1, and *Bam*HI-A rightward transcripts (BARTs)). The stably expressed housekeeping gene β_2-microglobulin (*β2M*) was used as an endogenous control and reference gene for relative quantification. Each experiment was conducted in triplicate and results are shown as the mean of three samples with standard errors.

Immunohistology and *in situ* hybridization

Tissue blocks were fixed with 10% buffered formalin, embedded in paraffin, and sectioned at 5 μm and stained with hematoxylin and eosin (HE). The monoclonal antibodies used were anti-CD3, anti-CD20, anti-follicular dendritic cell (FDC), EBNA2, LMP1 and BZFL1 (Dako), all of which were used after antigen retrieval following heating in a microwave oven [27,29]. *In situ* hybridization was performed using the EBER1 probe (Dako) as previously described [24,27]. Hybridization was detected using mouse monoclonal anti-fluorescein isothiocyanate (Dako) and a Vectastain ABC kit (Vector). For both immunostaining and *in situ* hybridization, diaminobenzidine was used for visualization.

Flow cytometry

At day 15–24 post-infection with EGFP-EBV, single-cell suspensions were dissected from tissue blocks by mechanical dissociation. Tissue blocks were placed into a petri plate with complete medium and gently ground with pestles. As shown previously, this procedure releases lymphocytes from stromal elements [23]. Similarly, cells that had emigrated into the collagen sponge were mechanically squeezed out and collected by centrifugation. Cell debris and fragments were removed and mononuclear cells (MNCs) were purified by Ficoll-Hypaque centrifugation [30]. MNCs were washed three times and stained using a combination of the following monoclonal antibodies (mAbs): phycoerythrin (PE)-labeled anti-CD19 (clone HD37; Dako); anti-CD3 (clone UCHT1; eBioscience); anti-CD56 (clone IM2073; Beckman Coulter); PE-cyanin 5 (PC5)-labeled anti-CD56 (clone IM2654; Beckman Coulter); and anti-HLA-DR (clone IMMU357; Beckman Coulter). In a few experiments, collected cells were also stained with 7-amino-actinomycinD (7-AAD; BD Pharmingen) at day 24, to exclude dead cells on samples. Discrimination between infection with memory or naive B cells was determined using the following antibody combination: PE-labeled anti-CD27 (clone M-T271; Becton Dickinson); anti-IgD (clone IgD26; Miltenyi Biotec); and PC5-labeled anti-CD19 (clone HIB19; eBioscience). Isotype-matched monoclonal mouse IgG antibodies were used in each experiment as controls. Stained cells were analyzed using FACSCalibur and CellQuest version 5.2.1 software (Becton Dickinson).

Acyclovir (ACV) treatment

To test the anti-EBV activity of ACV (GlaxoSmithKline), B95-infected tissue blocks were incubated with culture medium containing ACV at various concentrations (1.5, 5, 15 or 45 μg/ml). Culture medium was changed every 3 days after viral inoculation, and ACV was added with every medium change. A

sample of medium collected from each exchange was used for quantification of EBV DNA, as previously mentioned.

Flow cytometric in situ hybridization (FISH) assay

To quantify EBV-infected cells and to analyze the cell types of EBV-infected populations, FISH assays were used [31]. Briefly, 5×10^5 MNCs were stained with phycoerythrin cyanine 5 (PC5)-labeled anti-CD45 (clone HI30; Biolegend) monoclonal antibodies for 1 h at 4°C. Isotype-matched monoclonal mouse IgG antibodies were used as controls. After staining with antibodies, cells were fixed with 1% acetic acid/4% paraformaldehyde, permeabilized with 0.5% Tween 20/phosphate-buffered saline, and hybridized with a fluorescein-labeled EBER-specific peptide nucleic acid probe (Y5200; Dako). Fluorescence intensity was enhanced using the AlexaFluor 488 Signal Amplification Kit (Molecular Probes), and stained cells were analyzed using FACSCalibur and CellQuest software (BD Biosciences).

Statistical analyses

Data are presented as means ± standard error of the mean. Statistical analyses were conducted using StatView version 5.0

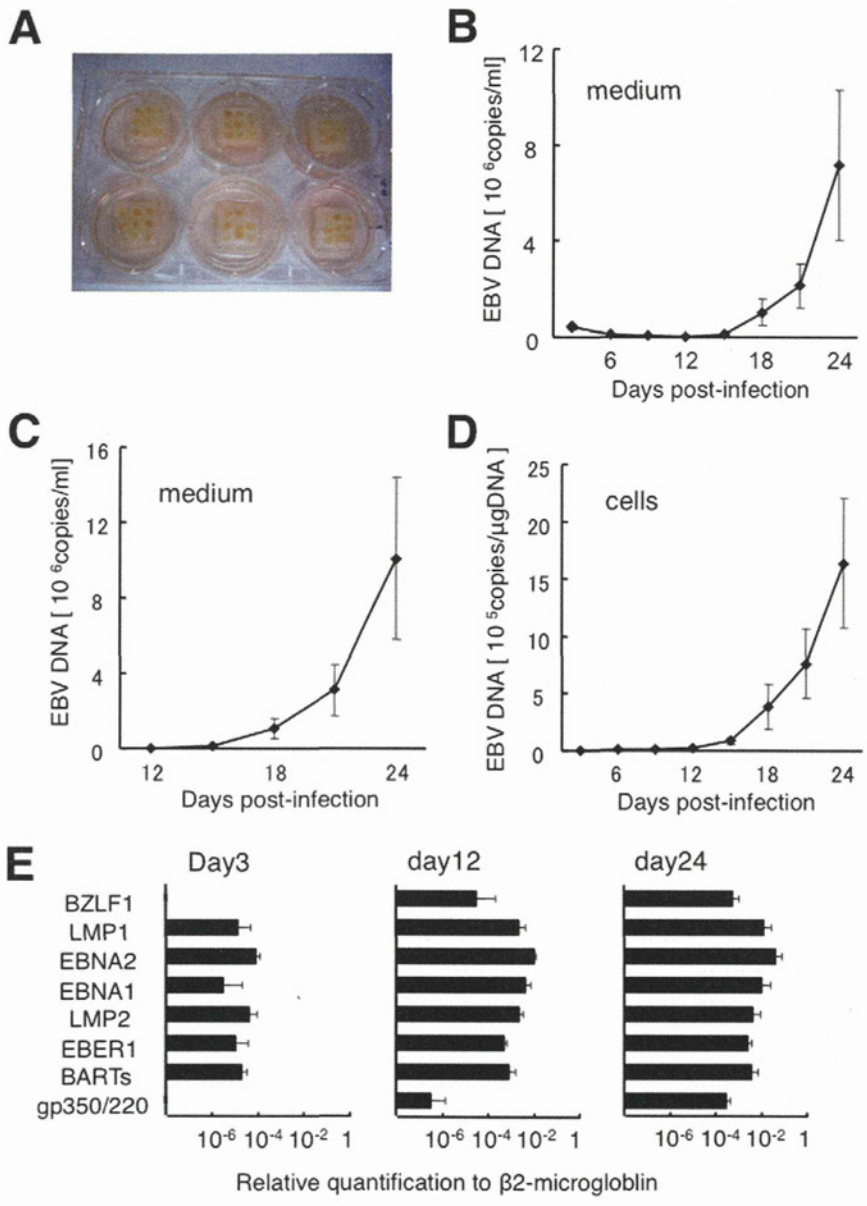

Figure 1. Kinetics of EBV DNA and expression patterns of EBV-related genes in human tonsil tissue explants infected with B95-8. Culture medium was changed every 3 days, and collected medium was centrifuged. Cell-free supernatants and cells collected from culture medium were used for quantification of EBV DNA by real-time PCR assay and quantification of viral mRNA by real-time RT-PCR assay. Data are presented as mean ± standard error of the mean. **A**) Tissue blocks on top of collagen sponge gels in a six-well plate. **B**) Kinetics of EBV DNA in cell-free supernatants. Average data were obtained from tissues derived from 12 donors. **C**) Plots of accumulated EBV DNA in cell-free culture medium after day 12 post-infection ($n=12$). **D**) Kinetics of EBV DNA in cells from medium ($n=12$). **E**) Levels of EBV-related gene expressions in cells at 3, 12, and 24 days post-infection ($n=4$).
doi:10.1371/journal.pone.0025490.g001

software (SAS Institute). The Kruskal-Wallis test was used to compare inhibition rates of EBV infection at each concentration of ACV. Values of $P<0.05$ were considered statistically significant.

Results

Replication of EBV B95–8 in human tonsil tissue explants

To establish a model system for the study of EBV infection, we tested the ability of B95–8 virus to replicate in human tonsillar tissue. The prepared tonsil tissue blocks (**Fig. 1A**) were exposed to B95–8, and cell-free supernatants and cells were collected. **Figure 1B** shows the kinetics of EBV DNA in culture supernatants of infected tissues at each time point. EBV DNA level gradually dropped and was minimal on day 12 post-infection, then steadily increased. When we applied the viral suspension on top of collagen sponge gels without tonsil tissues and changed the culture medium every 3 days, EBV DNA in culture medium gradually decreased and fell below the limit of detection by day 12 post-infection (data not shown). Kinetics before day 12 post-infection resemble those in EBV-infected tissue before day 12 post-infection, suggesting that EBV replication may become apparent after day 12 post-infection. We therefore showed the kinetics of EBV DNA in culture medium as a cumulative curve by totaling values from day 12 post-infection and after (**Fig. 1C**). Levels of viral DNA peaked between 1.3×10^5 and 4.3×10^7 (median, 4.1×10^6) genome-equivalents/ml of culture supernatant on day 24 post-infection ($n=12$). Increasing levels of EBV over time were also observed in cells from culture medium with peak levels between 1.2×10^4 and 6.7×10^6 (median, 8.0×10^5) genome-equivalents/μg of DNA at day 24 post-infection ($n=12$) (**Fig. 1D**).

Next, we analyzed expressions of eight EBV-associated genes in cells from culture medium using a real-time RT-PCR assay (**Fig. 1E**). Expression levels of all genes examined increased after day 12 post-infection ($n=4$). The immediate early gene BZLF1 was not detected on day 3 post-infection, but was detected after day 12 post-infection. In some series of experiments, we used RNA extracted from cells from dissected tissues and measured EBV gene expression. Expression patterns

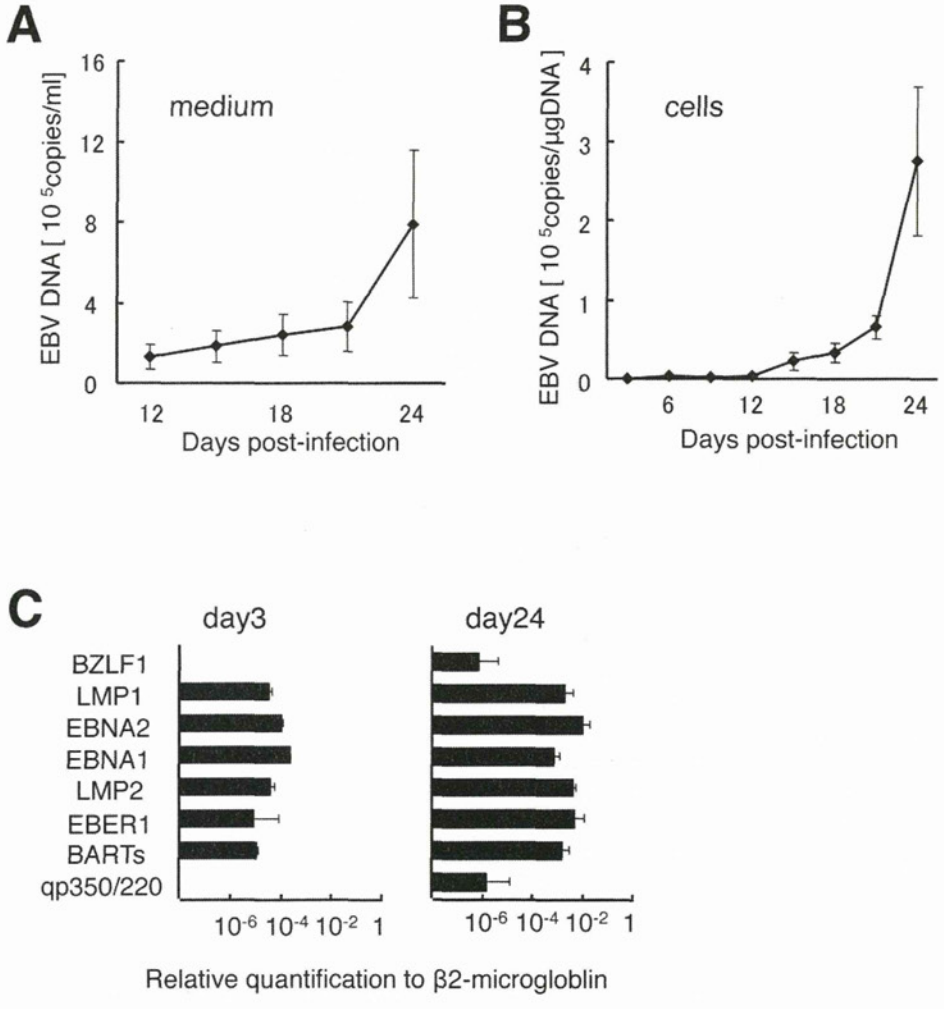

Figure 2. Kinetics of EBV DNA and expression patterns of EBV-related genes in human tonsil tissue explants infected with EGFP-EBV. Cell-free supernatants and cells collected from culture medium were used for quantification of EBV DNA by real-time PCR assay and quantification of viral mRNA by real-time RT-PCR assay. Data are presented as mean ± standard error of the mean. **A**) Plots of accumulated EBV DNA in cell-free culture medium after 12 days post-infection ($n=8$). **B**) Plots of accumulated EBV DNA in cells from medium ($n=2$). **C**) Levels of EBV-related genes expressions in cells at 3 and 24 days post-infection ($n=3$).
doi:10.1371/journal.pone.0025490.g002

of transcripts resembled those of cells collected from tissue blocks (data not shown).

Replication of recombinant EGFP-EBV in human tonsil tissue explants

We tested the ability of EGFP-EBV to replicate in human tonsil tissues in the same way as B95–8. Levels of EBV DNA in culture supernatants of EGFP-EBV-infected tissues as primary data were measured for each time point. EBV DNA levels gradually decreased and were minimal on days 12–15 post-infection, then steadily increased (data not shown). Productive infection was documented by the kinetics of EBV DNA accumulation in culture supernatants of infected tissues using real-time quantitative PCR (**Fig. 2A**), with peak levels between 2.1×10^4 and 2.5×10^6 genome-equivalents/ml of culture supernatant (median, 3.5×10^5 genome-equivalents/ml of culture supernatant) at day 24 post-infection in tissues infected with EGFP-EBV ($n=8$). Increasing levels of EBV over time were also detected by measuring cell-associated DNA (**Fig. 2B**), with peak levels between 1.4×10^5 and 4.1×10^5 genome-equivalents/μg DNA at day 24 post-infection ($n=2$).

Expressions of viral genes in cells collected from culture medium of EGFP-EBV infected tissues are shown in **Figure 2C**. Expressions of lytic cycle genes and increased levels of genes expression were subsequently observed at day 24 post-infection ($n=3$). Use of recombinant EGFP-EBV did not influence EBV gene expression compared to that in B95–8.

Histological analyses in EBV-infected human tonsil tissues

Histological analysis showed that tissues retained their gross morphology, even at day 24 post-infection (**Fig. 3A**, $n=4$). Immunohistochemical analysis performed by staining paraffin-embedded sections of tissue blocks with anti-CD3, anti-CD20, and anti-FDC mAbs revealed the presence of T cells (**Fig. 3B**), B cells (**Fig. 3C**), and FDCs (**Fig. 3D**). B cells were concentrated in follicular areas (**Fig. 3C**), while T cells (**Fig. 3B**) were confined to interfollicular areas. FDCs were detected in follicular areas (**Fig. 3D**). EBER-positive cells were detected, mainly in the interfollicular areas (**Fig. 3E**). EBER-positive cells represented a mixture of cells ranging from large lymphoid blasts to small lymphoid cells (**Fig. 3F**). No morphological evidence suggested EBV infection of cells other than lymphoid cells. BZLF1, a hallmark of lytic infection, was also detected in lymphoid cells (**Fig. 3G**), while EBNA2 and LMP1 were not detected in tissue samples.

Target cells of primary EBV infection in human tonsil tissues

To quantify and identify EBV-infected cells in tonsil tissues, we investigated the lineage of $EGFP^+$ cells prepared from tissue blocks infected with EGFP-EBV by flow cytometry using mAbs directed against several lymphocyte membrane antigens. GFP signals were not clearly detected before day 15, and the initial EBV-infected cells could not be determined (data not shown). Collected cells were stained with 7-AAD at day 24 in three experiments and 7-AAD-positive cells comprised $2.3\pm1.6\%$ of the lymphocyte population gated by standard forward and side scatter profiles (data not shown). **Figure 4A** shows a representative experiment with results ($n=4$) indicating that the majority of $EGFP^+$ cells were $CD19^+$ cells, with a very limited proportion of other types of lymphocytes. **Figure 4B** represents the kinetics in the proportion of $EGFP^+$ $CD19^+$ cells among all $CD19^+$ cells at 15–24 days post-infection ($n=4$). Mean proportions of $EGFP^+$ $CD19^+$ cells increased over time, with frequencies of $3.7\pm1.3\%$, $22.5\pm9.1\%$, $25.7\pm6.2\%$, and $40.8\pm11.3\%$ at days 15, 18, 21, and 24 day post-infection, respectively. These data indicate that EBV mainly infected B cells in tonsillar tissue explants. Furthermore, $EGFP^+$ cells were closely examined to determine the phenotype of EBV-infected cells. A representative result is shown in **Figure 5** ($n=2$). Most $EGFP^+$ cells were $CD3^-$ $CD56^-$ $CD19^+$ $HLA\text{-}DR^+$, and both naïve ($CD19^+IgD^+$, mean $22.6\pm6.0\%$ of $EGFP^+$ cells) and memory ($CD19^+$ $CD27^+$, mean $73.5\pm7.5\%$ of $EGFP^+$ cells) B cells were detected.

Inhibition of EBV replication by ACV in human tonsil tissues

Finally, we investigated the anti-EBV activity of ACV in infected tonsil tissues. Blocks of tonsil tissues were cultured with medium containing various concentrations of ACV. The amount

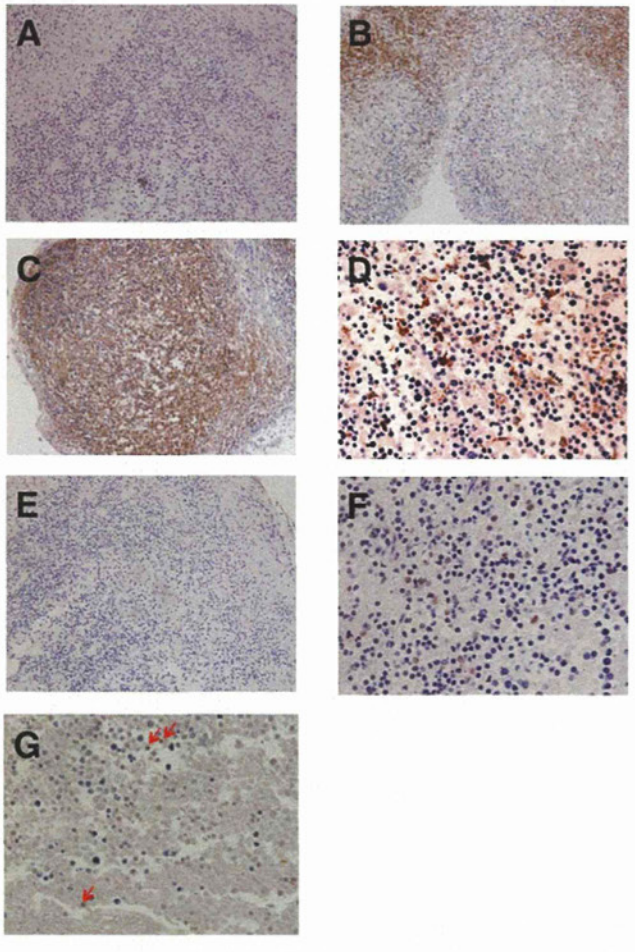

Figure 3. Histological analyses of tonsil tissues infected with B95–8 using immunostaining and *in situ* hybridization with EBER-RNA. Samples were obtained from EBV-infected tissues at 24 days post-infection. Pictures are representative of results from four experiments. **A**) Low-power view of tonsillar lymphoid tissue (HE stain). Magnification, ×100. **B**) Low-power view of $CD3^+$ lymphocytes in an interfollicular area (CD3 stain). Magnification, ×100. **C**) Low-power view of $CD20^+$ lymphocytes in a follicular area (CD20 stain). Magnification, ×100. **D**) High-power view of anti-follicular dendritic cell $(FDC)^+$ in a follicular area (anti-FDC stain). Magnification, ×400. **E**) Low-power view of $EBER^+$ lymphocytes (EBER ISH stain). Magnification, ×100. **F**) High-power view of $EBER^+$ lymphocytes in an interfollicular area (EBER ISH stain). Magnification, ×400. **G**) High-power view of $BZLF1^+$ lymphocytes (arrows) in an interfollicular area (BZLF1 stain). Magnification, ×400.
doi:10.1371/journal.pone.0025490.g003

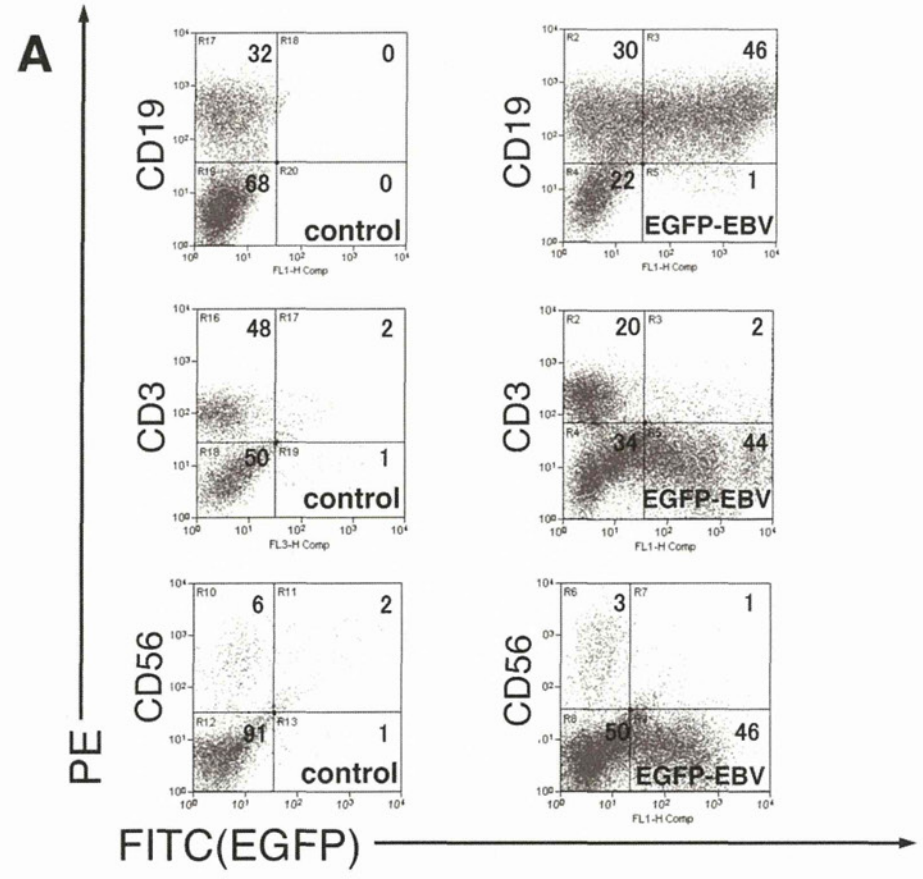

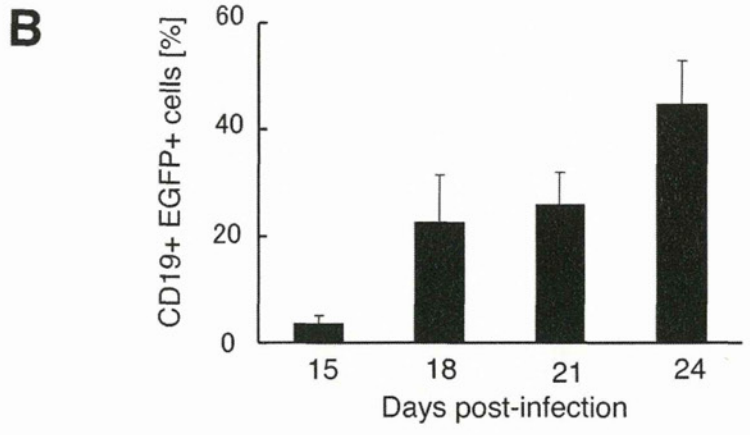

Figure 4. Phenotype of EGFP$^+$ cells in human tonsil tissue infected with EGFP-EBV. At 15–24 days post-infection, single cell suspensions were dissected from tissue blocks. Cells were stained with phycoerythrin (PE)-labeled anti-CD19, CD3, CD56 monoclonal antibodies, then analyzed by flow cytometry. **A**) A representative experiment is shown ($n = 4$). Density plots represent CD19, CD3, CD56 versus EGFP for control and EGFP-EBV-infected tissues at 24 days post-infection. Numbers in quadrants indicate percentages of lymphocytes for each surface immunophenotype. **B**) Mean proportion of EGFP$^+$ CD19$^+$ cells among CD19$^+$ cells at 15–24 days post-infection. Average data were obtained from 27 blocks of tissue derived from four donors. Results represent mean ± standard error of the mean. ctrl, control (uninfected tonsil tissues).
doi:10.1371/journal.pone.0025490.g004

of EBV DNA was measured in cell-free culture medium and in cells collected from culture medium. EBV replication was suppressed by ACV treatment in a dose-dependent manner (**Fig. 6A**). Mean accumulations of EBV DNA in culture medium at day 24 post-infection were $1.9\pm0.9\times10^5$, $5.7\pm3.1\times10^5$, $5.4\pm2.6\times10^5$, $9.9\pm5.3\times10^5$, and $2.6\pm1.4\times10^6$ genome-equivalents/ml in tissues treated with 45, 15, 5, 1.5, and 0 μg/ml of ACV, respectively ($n = 3$). Reduction rates in total production of EBV DNA accumulated in culture medium at day 24 post-infection were 90±4%, 76±7%, 77±3%, and 64±2% in tissues treated with 45, 15, 5, and 1.5 μg/ml of ACV ($P<0.01$), respectively. Suppression of EBV replication was also documented by measurement of EBV DNA in cells from culture medium (**Fig. 6B**). Mean levels of EBV DNA in these MNCs were $4.7\pm3.1\times10^4$, $8.7\pm5.2\times10^4$, $2.5\pm1.8\times10^4$, $2.7\pm1.8\times10^5$, and $6.9\pm3.9\times10^5$ genome-equivalents/μg DNA at day 24 post-

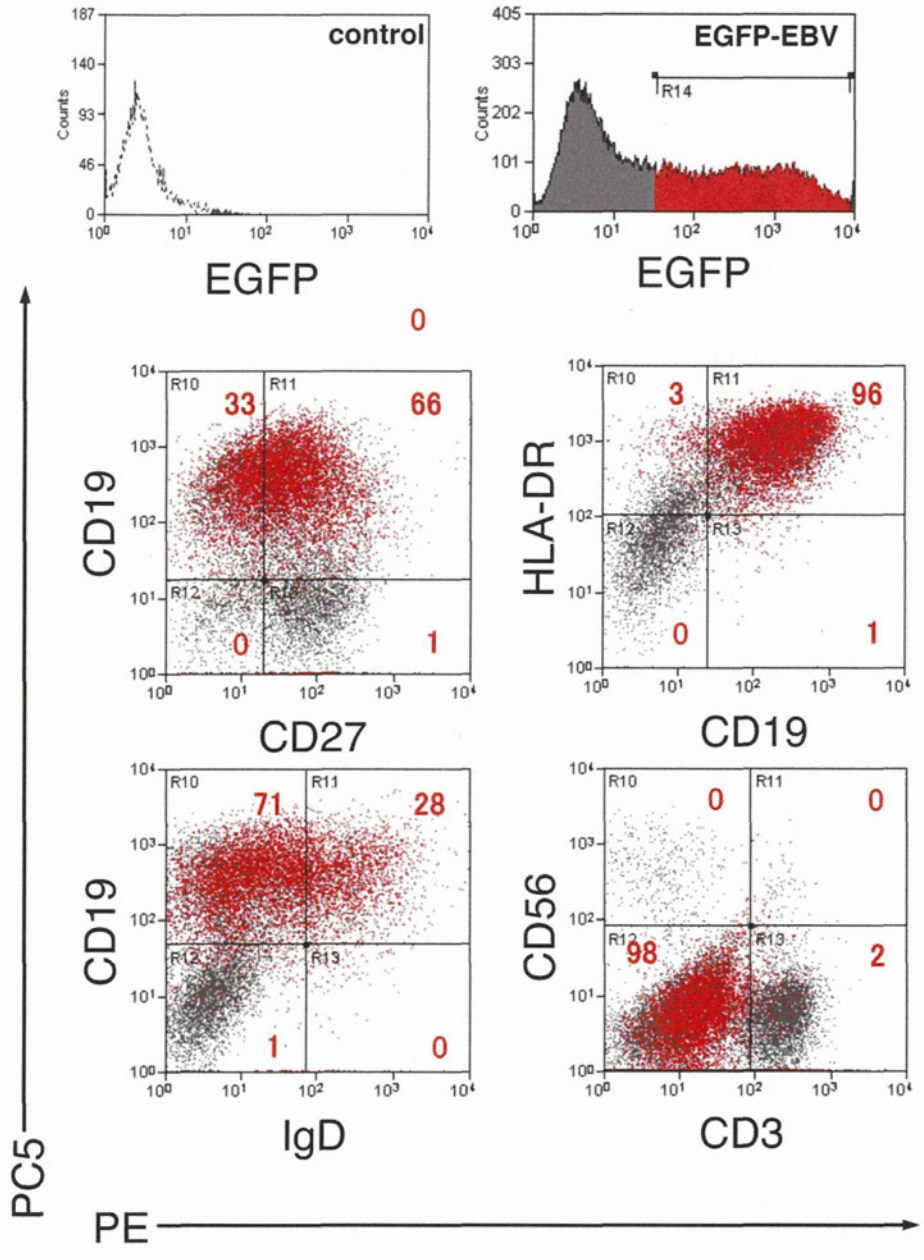

Figure 5. Phenotype of EGFP$^+$ cells in human tonsil tissue infected with EGFP-EBV using flow cytometry. Samples were obtained from EBV-infected tissues at 24 days post-infection. EGFP$^+$ (red) and EGFP$^-$ (grey) MNCs were gated and plotted on quadrants as PE-labeled and PC5-labeled surface antigens. A representative experiment is shown ($n = 2$). Numbers in quadrants indicate percentages of EGFP$^+$ lymphocytes for each surface immunophenotype.
doi:10.1371/journal.pone.0025490.g005

infection in tissues treated with 45, 15, 5, 1.5, and 0 μg/ml of ACV, respectively (n = 3). Moreover, the number of EBV-infected cells was compared in the presence or absence of ACV using FISH assay. The percentage of EBER$^+$ cells among CD45$^+$ cells was decreased at day 24 post-infection in a dose-dependent manner (10% with 45 μg/ml of ACV, 19% with 15 μg/ml, 24% with 5 μg/ml, and 32% without ACV, $n = 1$) (Fig. 6C).

Discussion

Viral infection models using human lymphoid tissues have the advantages of enabling culturing while maintaining tissue cytoarchitecture (including major lymphocyte subtypes and the follicular-dendritic cell network) and supporting productive virus infection without exogenous activation and stimulation. These models have been reported as useful for analyzing the pathogenicity of viruses that mainly infect lymphoid tissues [16]. In a study of the herpesvirus family, Grivel *et al.* used a tonsillar infection model to investigate cellular tropism and the pathogenic effects of HHV-6, demonstrating that HHV-6 infects efficiently without exogenous stimulation and that T-lymphocytes are the main cells infected [19]. The present study established an experimental EBV infection model with a culture system using tonsil tissues and confirmed that the amount of EBV-DNA in medium and in cells

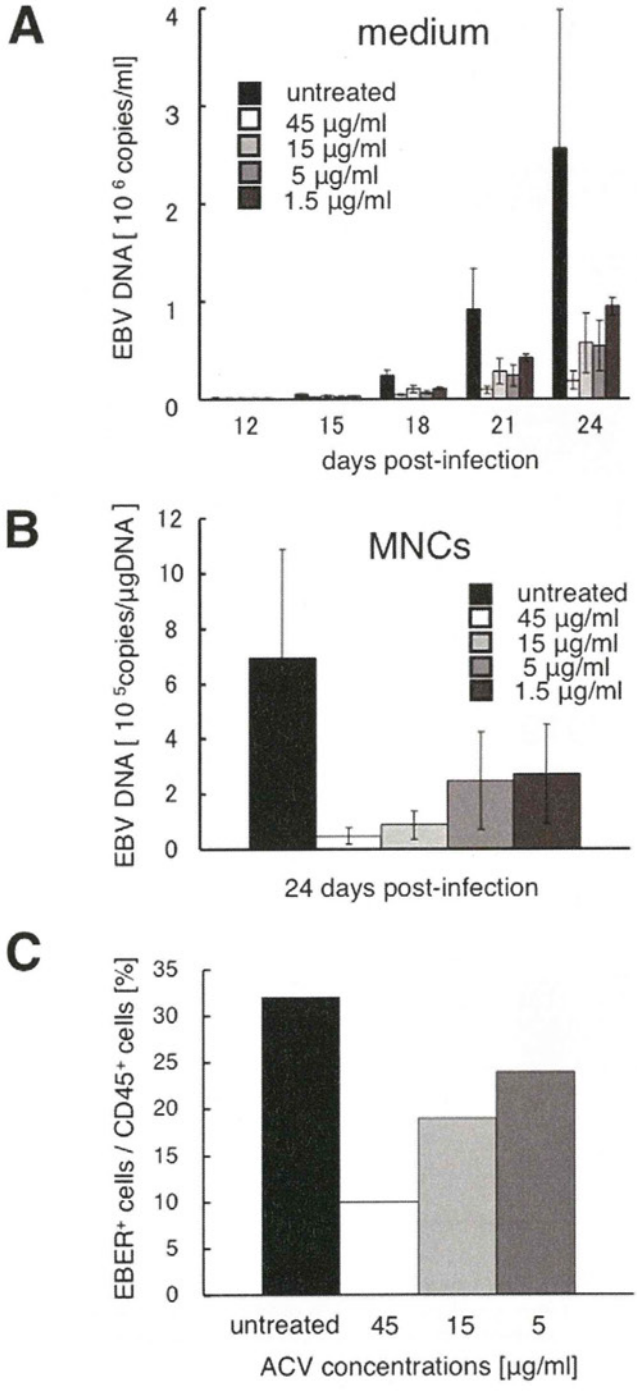

Figure 6. Inhibition by acyclovir (ACV) of EBV replication in human tonsillar tissues explants. Human tonsillar tissues were infected with B95–8 and treated with ACV at various concentrations. Antiviral activity of ACV was evaluated by comparing viral replication in ACV-treated tissues with that in untreated donor-matched control tissues. Data are presented as means ± standard errors of mean. **A**) Kinetics of EBV replication were measured by real-time PCR assay for viral DNA in culture medium ($n = 3$). **B**) EBV DNA was quantified in cells at 24 days post-infection ($n = 3$). **C**) Comparison of the number of EBV-infected cells in the presence or absence of ACV at 24 days post-infection using FISH assay ($n = 1$).
doi:10.1371/journal.pone.0025490.g006

increased over time. The increase in DNA in this infection model was pronounced from ≥12 days post-infection, with the amount of virus starting to increase later using EBV than in tonsillar infection models using HHV-6 or HHV-7 [18,19]. This was not regarded as a problem with the tonsillar infection model, but rather as resulting from differences in viral proliferation; however, establishment of an EBV infection model may be more difficult for this reason. Yajima *et al.* infected humanized NOG mice intravenously with EBV and reported that EBV-DNA in blood increased after 3–4 weeks [15]. Changes in the amount of DNA in our infection model were not inconsistent with those results. We also investigated expression of EBV-related genes in cells obtained from our infection model, revealing expression of lytic genes and increased levels of gene transcripts over time, in addition to latent genes expressed as latency type III. These data show that EBV produces both latent and productive infections in a tonsillar infection model. Several histological studies of IM tonsils have shown the presence of B cells expressing latency types III, II, and I, as well as lytic genes [32,33]. In the present EBV-infection model, EBV *de novo* synthesis was not shown directly. However, several results suggested that at least some of the infected cells in this model gave rise to progeny virus: (1) the amount of EBV DNA in both culture media and cells markedly increased after day 12 post-infection, (2) immediate early gene BZLF1 was detected in lymphoid cells both in the immunohistochemical analysis and in the quantification of mRNA expression, and (3) ACV treatment reduced the levels of EBV DNA. This model may represent early events in primary EBV infection, before the emergence of IM symptoms, rather than a stable latent infection. Taken together, the tonsillar infection model is useful for analyzing the pathology of primary infection with EBV.

EBV is believed to be transmitted orally at oropharyngeal sites [34]. For this reason, numerous histological studies of IM tonsils have examined viral-cell interactions during primary infection [32,35,36]. These investigations have been unable to detect EBV infection of the tonsillar epithelium, with most reports stating that the main infected cells are B cells [32,35,36,37]. Our histological analysis also suggested B-cell infection. Flow cytometric analysis also showed that B cells were mainly infected, supporting the findings of previous studies. The events involved in virus colonization of the B-cell system during primary infection remain poorly understood. Various studies have looked at tonsillar EBV-infected B-cell subsets in healthy virus carriers [38,39,40]. Joseph *et al.* used IgD mAb from the tonsils of healthy virus carriers to sort each B-cell subset and performed limiting-dilution DNA PCR on each subset, detecting EBV in both naïve (IgD^+) and memory B cells [38].

Meanwhile, the only report on EBV-infected B-cell subsets in tonsils obtained from patients with IM has been the recent study by Chaganti *et al.* [36]. They sorted each B-cell subset using CD27, IgD, and CD38 mAbs from tonsils they obtained and performed quantitative PCR on each subset, reporting that the amount of DNA was greatest in $CD38^+$ cells, followed by memory cells ($CD27^+$) and finally naïve (IgD^+ $CD27^-$) B cells. We investigated the lineage of $EGFP^+$ cells dissected from tissue blocks infected with EGFP-EBV by flow cytometry using mAbs directed against several lymphocyte membrane antigens and the proportion of EBV-infected B cells was higher among memory cells ($CD27^+$) than among naïve cells (IgD^+), consistent with findings from the above study. This showed that the tonsillar infection model is useful for analyzing EBV-infected lymphocyte subsets. Further observation of changes in subsets over time as well as of additional surface or intracellular molecules, such as cell adhesion markers

and chemokine receptors, will enable us to characterize and examine the function of EBV-infected cells.

Conversely, tissue culture models show a number of limitations. The first is that wide differences in proliferative capacity within tissue exist between donors. In practice, even when experiments have been performed under the same protocol, differences of around 100-fold have occurred in amounts of DNA between tissues. The same phenomenon has also been observed in tonsillar infection models using other viruses [19,41]. This is probably because the structure and cell composition of tonsil tissue vary greatly among donors. The second limitation that can be raised is that tissues deteriorate as a result of long-term culture. We cultured cells for 4 weeks, but regarded culture for longer than this period as difficult due to deteriorations observed in tissue samples. Histological investigation of tissue segments also showed that although the structures were maintained, the number of lymphocytes decreased significantly. The third limitation is that investigation of EBV-specific immune responses was difficult in this model. Symptoms of IM are believed to be closely related to the specific immune responses of the host to EBV infection [1]. With respect to specific immune response in tonsillar infection models, antibody response to antigen load with antigens such as diphtheria and tetanus toxoids has been reported [42]. However, IM symptoms appear as late as 4–6 weeks after viral transmission *in vivo* [2]. Since tissue deterioration makes culture for longer periods than this difficult, evaluation of specific immune responses was considered difficult.

Treatment of IM and PTLD with regular antiviral agents is not recommended [1], but antiviral agents may be required in cases such as immunocompromised patients with severe IM or HIV-infected patients with oral hairy leukoplakia, and novel antiviral agents need to be developed for treatment in such cases. ACV is known to be a guanosine nucleoside analog with activity against several types of α-herpesvirus. ACV inhibits virus-associated DNA polymerase, suppressing virus replication. Although some reports have indicated that ACV is effective against EBV *in vitro* [43,44], clear efficacy in actual clinical practice has not been established [1,2]. Using the tonsillar infection model, we showed that ACV exerts a dose-dependent antiviral action. For previous evaluations of *in vitro* efficacy, EBV-infected cell suspension cultures have been used [43,44]. Actual EBV infection, however, occurs in the oropharyngeal lymphoid tissues [2,34], so use of a tonsillar infection model may more closely reproduce the *in vivo* environment. The tonsillar infection model was also regarded as applicable to the screening of novel antiviral agents.

In this study, we established an EBV infection model using human tonsil tissues. EBV infection and proliferation in this model could be observed without the need for any special exogenous stimulation. Use of flow cytometry also enabled qualitative and quantitative analysis of infected cells. This model has potential for use in the pathological analysis of local tissues at the time of primary infection, as well as for screening novel antiviral agents.

Acknowledgments

The authors wish to thank H. Yamada, M. Miyake and S. Kumagai for technical assistance, and Y. Ushijima for technical suggestions and instructions. We are also grateful to F. Ando for secretarial assistance.

Author Contributions

Conceived and designed the experiments: YI HK. Performed the experiments: KG YI SI FG S. Nakamura. Analyzed the data: KG YI. Contributed reagents/materials/analysis tools: SM KT TM MT S. Nakata TN. Wrote the paper: KG YI.

References

1. Cohen JI (2000) Epstein-Barr virus infection. N Engl J Med 343: 481–492.
2. Alan B. Rickinson EK (2007) Epstein-Barr virus. In: David M.Knipe PMH, ed. Fields Virology Fifth ed. Philadelphia, PA: Lippincott Williams & Wilkins. pp 2655–2700.
3. Johannessen I, Crawford DH (1999) In vivo models for Epstein-Barr virus (EBV)-associated B cell lymphoproliferative disease (BLPD). Rev Med Virol 9: 263–277.
4. Woodford NL, Call DR, Remick DG, Rochford R (2004) Model of angiogenesis in mice with severe combined immunodeficiency (SCID) and xenoengrafted with Epstein-Barr virus-transformed B cells. Comp Med 54: 209–215.
5. Pegtel DM, Middeldorp J, Thorley-Lawson DA (2004) Epstein-Barr virus infection in ex vivo tonsil epithelial cell cultures of asymptomatic carriers. J Virol 78: 12613–12624.
6. Hong GK, Gulley ML, Feng WH, Delecluse HJ, Holley-Guthrie E, et al. (2005) Epstein-Barr virus lytic infection contributes to lymphoproliferative disease in a SCID mouse model. J Virol 79: 13993–14003.
7. Takashima K, Ohashi M, Kitamura Y, Ando K, Nagashima K, et al. (2008) A new animal model for primary and persistent Epstein-Barr virus infection: human EBV-infected rabbit characteristics determined using sequential imaging and pathological analysis. J Med Virol 80: 455–466.
8. Traggiai E, Chicha L, Mazzucchelli L, Bronz L, Piffaretti JC, et al. (2004) Development of a human adaptive immune system in cord blood cell-transplanted mice. Science 304: 104–107.
9. Gimeno R, Weijer K, Voordouw A, Uittenbogaart CH, Legrand N, et al. (2004) Monitoring the effect of gene silencing by RNA interference in human CD34+ cells injected into newborn RAG2−/− gammac−/− mice: functional inactivation of p53 in developing T cells. Blood 104: 3886–3893.
10. Islas-Ohlmayer M, Padgett-Thomas A, Domiati-Saad R, Melkus MW, Cravens PD, et al. (2004) Experimental infection of NOD/SCID mice reconstituted with human CD34+ cells with Epstein-Barr virus. Journal of virology 78: 13891–13900.
11. Ishikawa F, Yasukawa M, Lyons B, Yoshida S, Miyamoto T, et al. (2005) Development of functional human blood and immune systems in NOD/SCID/IL2 receptor {gamma} chain(null) mice. Blood 106: 1565–1573.
12. Shultz LD, Lyons BL, Burzenski LM, Gott B, Chen X, et al. (2005) Human lymphoid and myeloid cell development in NOD/LtSz-scid IL2R gamma null mice engrafted with mobilized human hemopoietic stem cells. Journal of immunology 174: 6477–6489.
13. Strowig T, Gurer C, Ploss A, Liu YF, Arrey F, et al. (2009) Priming of protective T cell responses against virus-induced tumors in mice with human immune system components. J Exp Med 206: 1423–1434.
14. Melkus MW, Estes JD, Padgett-Thomas A, Gatlin J, Denton PW, et al. (2006) Humanized mice mount specific adaptive and innate immune responses to EBV and TSST-1. Nature medicine 12: 1316–1322.
15. Yajima M, Imadome K, Nakagawa A, Watanabe S, Terashima K, et al. (2008) A new humanized mouse model of Epstein-Barr virus infection that reproduces persistent infection, lymphoproliferative disorder, and cell-mediated and humoral immune responses. J Infect Dis 198: 673–682.
16. Grivel JC, Margolis L (2009) Use of human tissue explants to study human infectious agents. Nat Protoc 4: 256–269.
17. Lisco A, Vanpouille C, Tchesnokov EP, Grivel JC, Biancotto A, et al. (2008) Acyclovir is activated into a HIV-1 reverse transcriptase inhibitor in herpesvirus-infected human tissues. Cell Host Microbe 4: 260–270.
18. Lisco A, Grivel JC, Biancotto A, Vanpouille C, Origgi F, et al. (2007) Viral interactions in human lymphoid tissue: Human herpesvirus 7 suppresses the replication of CCR5-tropic human immunodeficiency virus type 1 via CD4 modulation. J Virol 81: 708–717.
19. Grivel JC, Santoro F, Chen S, Faga G, Malnati MS, et al. (2003) Pathogenic effects of human herpesvirus 6 in human lymphoid tissue ex vivo. J Virol 77: 8280–8289.
20. Maruo S, Yang L, Takada K (2001) Roles of Epstein-Barr virus glycoproteins gp350 and gp25 in the infection of human epithelial cells. J Gen Virol 82: 2373–2383.
21. Condit RC (2007) Principles of virology. In: David M. Knipe PMH, ed. Fields Virology Fifth ed. 5th ed. Philadelphia, PA: Lippincott Williams & Wilkins. pp 25–57.
22. Glushakova S, Baibakov B, Margolis LB, Zimmerberg J (1995) Infection of human tonsil histocultures: a model for HIV pathogenesis. Nat Med 1: 1320–1322.
23. Glushakova S, Baibakov B, Zimmerberg J, Margolis LB (1997) Experimental HIV infection of human lymphoid tissue: correlation of CD4+ T cell depletion and virus syncytium-inducing/non-syncytium-inducing phenotype in histocultures inoculated with laboratory strains and patient isolates of HIV type 1. AIDS Res Hum Retroviruses 13: 461–471.
24. Kimura H, Morita M, Yabuta Y, Kuzushima K, Kato K, et al. (1999) Quantitative analysis of Epstein-Barr virus load by using a real-time PCR assay. J Clin Microbiol 37: 132–136.

25. Kimura H, Hoshino Y, Kanegane H, Tsuge I, Okamura T, et al. (2001) Clinical and virologic characteristics of CAEBV. Blood 98: 280–286.
26. Wada K, Kubota N, Ito Y, Yagasaki H, Kato K, et al. (2007) Simultaneous quantification of Epstein-Barr virus, cytomegalovirus, and human herpesvirus 6 DNA in samples from transplant recipients by multiplex real-time PCR assay. J Clin Microbiol 45: 1426–1432.
27. Kubota N, Wada K, Ito Y, Shimoyama Y, Nakamura S, et al. (2008) One-step multiplex real-time PCR assay to analyse the latency patterns of Epstein-Barr virus infection. J Virol Methods 147: 26–36.
28. Iwata S, Wada K, Tobita S, Gotoh K, Ito Y, et al. (2010) Quantitative analysis of Epstein-Barr virus (EBV)-related gene expression in patients with chronic active EBV infection. J Gen Virol 91: 42–50.
29. Nakamura S, Nagahama M, Kagami Y, Yatabe Y, Takeuchi T, et al. (1999) Hodgkin's disease expressing follicular dendritic cell marker CD21 without any other B-cell marker: a clinicopathologic study of nine cases. The American journal of surgical pathology 23: 363–376.
30. Johnston A, Sigurdardottir SL, Ryon JJ (2009) Isolation of mononuclear cells from tonsillar tissue. Curr Protoc Immunol Chapter 7: Unit 7 8.
31. Kimura H, Miyake K, Yamauchi Y, Nishiyama K, Iwata S, et al. (2009) Identification of Epstein-Barr virus (EBV)-infected lymphocyte subtypes by flow cytometric in situ hybridization in EBV-associated lymphoproliferative diseases. J Infect Dis 200: 1078–1087.
32. Niedobitek G, Agathanggelou A, Herbst H, Whitehead L, Wright DH, et al. (1997) Epstein-Barr virus (EBV) infection in infectious mononucleosis: virus latency, replication and phenotype of EBV-infected cells. J Pathol 182: 151–159.
33. Kurth J, Spieker T, Wustrow J, Strickler GJ, Hansmann LM, et al. (2000) EBV-infected B cells in infectious mononucleosis: viral strategies for spreading in the B cell compartment and establishing latency. Immunity 13: 485–495.
34. Thorley-Lawson DA (2005) EBV the prototypical human tumor virus–just how bad is it? J Allergy Clin Immunol 116: 251–261; quiz 262.
35. Anagnostopoulos I, Hummel M, Kreschel C, Stein H (1995) Morphology, immunophenotype, and distribution of latently and/or productively Epstein-Barr virus-infected cells in acute infectious mononucleosis: implications for the interindividual infection route of Epstein-Barr virus. Blood 85: 744–750.
36. Chaganti S, Heath EM, Bergler W, Kuo M, Buettner M, et al. (2009) Epstein-Barr virus colonization of tonsillar and peripheral blood B-cell subsets in primary infection and persistence. Blood 113: 6372–6381.
37. Trempat P, Tabiasco J, Andre P, Faumont N, Meggetto F, et al. (2002) Evidence for early infection of nonneoplastic natural killer cells by Epstein-Barr virus. J Virol 76: 11139–11142.
38. Joseph AM, Babcock GJ, Thorley-Lawson DA (2000) Cells expressing the Epstein-Barr virus growth program are present in and restricted to the naive B-cell subset of healthy tonsils. J Virol 74: 9964–9971.
39. Babcock GJ, Hochberg D, Thorley-Lawson AD (2000) The expression pattern of Epstein-Barr virus latent genes in vivo is dependent upon the differentiation stage of the infected B cell. Immunity 13: 497–506.
40. Laichalk LL, Hochberg D, Babcock GJ, Freeman RB, Thorley-Lawson DA (2002) The dispersal of mucosal memory B cells: evidence from persistent EBV infection. Immunity 16: 745–754.
41. Ito Y, Grivel JC, Chen S, Kiselyeva Y, Reichelderfer P, et al. (2004) CXCR4-tropic HIV-1 suppresses replication of CCR5-tropic HIV-1 in human lymphoid tissue by selective induction of CC-chemokines. J Infect Dis 189: 506–514.
42. Glushakova S, Grivel JC, Fitzgerald W, Sylwester A, Zimmerberg J, et al. (1998) Evidence for the HIV-1 phenotype switch as a causal factor in acquired immunodeficiency. Nat Med 4: 346–349.
43. Allaudeen HS, Descamps J, Sehgal RK (1982) Mode of action of acyclovir triphosphate on herpesviral and cellular DNA polymerases. Antiviral Res 2: 123–133.
44. Long MC, Bidanset DJ, Williams SL, Kushner NL, Kern ER (2003) Determination of antiviral efficacy against lymphotropic herpesviruses utilizing flow cytometry. Antiviral Res 58: 149–157.

VOLUME 29 · NUMBER 33 · NOVEMBER 20 2011

JOURNAL OF CLINICAL ONCOLOGY

ORIGINAL REPORT

Phase II Study of SMILE Chemotherapy for Newly Diagnosed Stage IV, Relapsed, or Refractory Extranodal Natural Killer (NK)/T-Cell Lymphoma, Nasal Type: The NK-Cell Tumor Study Group Study

Motoko Yamaguchi, Yok-Lam Kwong, Won Seog Kim, Yoshinobu Maeda, Chizuko Hashimoto, Cheolwon Suh, Koji Izutsu, Fumihiro Ishida, Yasushi Isobe, Eisaburo Sueoka, Junji Suzumiya, Takao Kodama, Hiroshi Kimura, Rie Hyo, Shigeo Nakamura, Kazuo Oshimi, and Ritsuro Suzuki

Motoko Yamaguchi, Mie University Graduate School of Medicine, Tsu; Yoshinobu Maeda, Okayama University Graduate School of Medicine, Okayama; Chizuko Hashimoto, Kanagawa Cancer Center, Yokohama; Koji Izutsu, NTT Medical Center Tokyo; Yasushi Isobe and Kazuo Oshimi, Juntendo University School of Medicine, Tokyo; Fumihiro Ishida, Shinshu University School of Medicine, Matsumoto; Eisaburo Sueoka, Saga University School of Medicine, Saga; Junji Suzumiya, Fukuoka University Chikushi Hospital, Fukuoka; Takao Kodama, Miyazaki University School of Medicine, Miyazaki; Hiroshi Kimura, Rie Hyo, Shigeo Nakamura, and Ritsuro Suzuki, Nagoya University Graduate School of Medicine, Nagoya, Japan; Yok-Lam Kwong, Queen Mary Hospital, University of Hong Kong, Hong Kong, China; Won Seog Kim, Samsung Medical Center, Sungkyunkwan University School of Medicine; Cheolwon Suh, Asan Medical Center, University of Ulsan College of Medicine, Seoul, Korea; and Kazuo Oshimi, Eisai Research Institute of Boston, Andover, MA.

Submitted February 25, 2011; accepted July 28, 2011; published online ahead of print at www.jco.org on October 11, 2011.

Supported by a Grant-in-Aid for Cancer Research from the Ministry of Health, Labor and Welfare of Japan.

Authors' disclosures of potential conflicts of interest and author contributions are found at the end of this article.

Clinical Trials repository link available on JCO.org.

Corresponding author: Ritsuro Suzuki, MD, PhD, Department of HSCT Data Management & Biostatistics, Nagoya University, Graduate School of Medicine, 1-1-20 Daiko-Minami, Higashi-ku, Nagoya, 461-0047 Japan; e-mail: r-suzuki@med.nagoya-u.ac.jp.

0732-183X/11/2933-4410/$20.00

DOI: 10.1200/JCO.2011.35.6287

ABSTRACT

Purpose
To explore a more effective treatment for newly diagnosed stage IV, relapsed, or refractory extranodal natural killer/T-cell lymphoma, nasal type (ENKL), we conducted a phase II study of the steroid (dexamethasone), methotrexate, ifosfamide, L-asparaginase, and etoposide (SMILE) regimen.

Patients and Methods
Patients with newly diagnosed stage IV, relapsed, or refractory disease and a performance status of 0 to 2 were eligible. Two cycles of SMILE chemotherapy were administered as the protocol treatment. The primary end point was the overall response rate (ORR) after the protocol treatment.

Results
A total of 38 eligible patients were enrolled. The median age was 47 years (range, 16 to 67 years), and the male:female ratio was 21:17. The disease status was newly diagnosed stage IV in 20 patients, first relapse in 14 patients, and primary refractory in four patients. The eligibility was revised to include lymphocyte counts of 500/μL or more because the first two patients died from infections. No treatment-related deaths were observed after the revision. The ORR and complete response rate after two cycles of SMILE chemotherapy were 79% (90% CI, 65% to 89%) and 45%, respectively. In the 28 patients who completed the protocol treatment, 19 underwent hematopoietic stem-cell transplantation. The 1-year overall survival rate was 55% (95% CI, 38% to 69%). Grade 4 neutropenia was observed in 92% of the patients. The most common grade 3 or 4 nonhematologic complication was infection (61%).

Conclusion
SMILE chemotherapy is an effective treatment for newly diagnosed stage IV, relapsed or refractory ENKL. Myelosuppression and infection during the treatment should be carefully managed.

J Clin Oncol 29:4410-4416. © 2011 by American Society of Clinical Oncology

INTRODUCTION

Extranodal natural killer (NK)/T-cell lymphoma, nasal type (ENKL), is a lymphoma associated with the Epstein-Barr virus (EBV), which is much more common in Asia and Latin America than in Western countries.[1,2] More than two thirds of patients with ENKL have stage I or II disease in the upper aerodigestive tract.[3-6] The prognosis for localized ENKL has been improving as a result of the use of either concurrent chemoradiotherapy[7,8] or chemotherapy with sandwiched radiotherapy.[9] In contrast, most patients with newly diagnosed stage IV, relapsed, or refractory ENKL treated with conventional chemotherapy designed for aggressive lymphomas, such as cyclophosphamide, doxorubicin, vincristine, and prednisone, survive for less than a year.[6] The poor outcome is partly because ENKL tumor cells express P-glycoprotein, which results in tumor multidrug resistance.[10-12] There are a number of long-term survivors among patients with advanced-stage, relapsed, or refractory ENKL who have undergone hematopoietic stem-cell transplantation (HSCT).[13-15] However, patients who received HSCT in complete response (CR) showed better prognosis than those who received HSCT during non CR. Therefore, the development of an effective chemotherapy for these patients is an important initial step in improving treatment outcomes.

Table 1. SMILE Chemotherapy

Agent	Dose/d	Route	Day
Methotrexate	2 g/m^2*	IV (6 hours)	1
Leucovorin	15 mg × 4	IV or PO	2, 3, 4
Ifosfamide	1,500 mg/m^2	IV	2, 3, 4
Mesna	300 mg/m^2 × 3	IV	2, 3, 4
Dexamethasone	40 mg/d	IV or PO	2, 3, 4
Etoposide	100 mg/m^2*	IV	2, 3, 4
L-asparaginase (*Escherichia coli*)	6,000 U/m^2	IV	8, 10, 12, 14, 16, 18, 20
G-CSF		SC or IV	Day 6 to WBC > 5,000/μL

NOTE. Cycles were repeated every 28 days. Two courses were planned as the protocol treatment.
Abbreviations: G-CSF, granulocyte-colony stimulating factor; IV, intravenously; PO, orally; SC, subcutaneous injection; SMILE, steroid (dexamethasone), methotrexate, ifosfamide, L-asparaginase, and etoposide.
*The recommended dose was determined in the preceding phase I study.

To explore the possibility of more effective induction chemotherapy for NK-cell neoplasms, the NK-Cell Tumor Study Group, comprising Japanese and Asian hematologists, has formulated a novel chemotherapeutic regimen: steroid (dexamethasone), methotrexate, ifosfamide, L-asparaginase, and etoposide (SMILE). These agents are multidrug resistance independent and may be key drugs for NK-cell neoplasms or for EBV-associated disease. From the phase I trial of SMILE, the recommended doses of methotrexate and etoposide were determined.[16] The CR rate in the phase I trial was 50% (three of six eligible patients), and the overall response rate (ORR) was 67% (four of six patients). To further evaluate the efficacy of SMILE chemotherapy, we conducted a subsequent phase II study.

PATIENTS AND METHODS

Eligibility Criteria

Patients with newly diagnosed stage IV, relapsed, or refractory disease who had undergone first-line chemotherapy were eligible. Those with aggressive NK-cell leukemia were excluded because no patients with aggressive NK-cell leukemia had been enrolled in the prior phase I study.[16] Patients who had received autologous HSCT more than 12 months before registration were also eligible. The other inclusion and exclusion criteria for the study were the same as those for the prior phase I study.[16] Briefly, patients from 15 to 69 years of age with a performance status of 0 to 2, based on the Eastern Cooperative Oncology Group scale, and preserved organ functions were included. Neither chemotherapy nor radiotherapy was administered within 21 days before registration. Patients who had clinical symptoms of CNS involvement were excluded.

The pretreatment staging procedures included a physical examination, a bone marrow aspiration and/or biopsy, a chest radiograph, and a computed tomography scan of the nasal cavity, neck, chest, abdomen, and pelvis. An endoscopy of the upper gastrointestinal tract and a positron emission tomography scan were recommended but not mandatory.

After patient enrollment, hematoxylin-eosin–stained sections were histologically reviewed by the Central Pathology Review Board based on the WHO classification.[1] Immunohistochemical staining was performed at the central pathology office using formalin-fixed, paraffin-embedded sections with antibodies against CD3, CD20, CD56, perforin, and granzyme B. In addition, in situ hybridization for EBV-encoded small RNA-1 was performed.

Registration of patients was conducted by facsimile between the participating physicians and the Center for Supporting Hematology-Oncology Trials Data Center (Nagoya, Japan). The study was approved by both the protocol review committee and the institutional review board of each institution. Written informed consent was obtained from all of the patients. The study was registered to the University Hospital Medical Information Network Clinical Trials Registry.

Treatment

SMILE chemotherapy was administrated as indicated in Table 1. On the basis of the results of the phase I trial,[16] administration of granulocyte colony-stimulating factor was mandatory from day 6 and discontinued if the leukocyte count exceeded 5,000/μL after the nadir phase. Antibiotic prophylaxis of sulfamethoxazole-trimethoprim was recommended. The criteria for the initiation of a second course of SMILE were as follows (1): a total of 4 weeks or more had passed since the prior course; (2) all of the following were achieved at least 1 day before the second course of SMILE: a leukocyte count of $\geq$ 2,000/μL, a platelet count of $\geq$ 100,000/μL, AST and ALT levels $\leq$ 5× the upper limit of normal, total bilirubin of $\leq$ 2.0 mg/dL, or serum creatinine of $\leq$ 1.5 mg/dL; and (3) there were no other symptoms or complications that were not suitable for the initiation of a second course. If there was no recovery 4 weeks after the day of the scheduled second course, the protocol treatment was terminated. Two courses of SMILE chemotherapy were planned for the protocol treatment. After the planned two courses, patients could undergo additional courses of SMILE and/or other chemotherapy, with or without autologous/allogeneic HSCT. The decision was made according to the discretion of treating physicians mainly on the basis of the patient's age, conditions, and the availability of HSC donors.

Response and Toxicity Criteria

The responses were assessed by the Central Imaging Review Board according to criteria modified from the WHO response criteria[17] that were also used in the prior phase I study of SMILE chemotherapy.[16] All of the examinations for restaging were done within 4 to 6 weeks (from day 22 to day 42) of the second course of SMILE. Because ENKL frequently occurs in the nasal/paranasal sites and leaves scar or necrotic tissue, it is sometimes difficult to determine whether or not a patient strictly attains CR using the WHO response criteria[17] or the International Workshop criteria.[18] Therefore, in this trial, CR was defined as the complete disappearance of all objective signs of disease, including enlarged lymph nodes or hepatomegaly and splenomegaly at the restaging. Partial response (PR) was defined as at least a 50% reduction of tumor volume without the occurrence of new lesions at the restaging. Progressive disease was defined as a greater than 25% increase in the sum of tumor lesions or the emergence of one or more new lesion(s) or clinical symptoms that indicate disease progression, such as "B" symptoms or elevated serum lactate dehydrogenase levels. No response was defined as any response that did not fall into the other defined categories. If a patient died before day 42 of the second course of SMILE and could not undergo the defined restaging procedure, the patient's response was recorded as early death. The ORR rate was defined as the proportion of all patients who were able to be evaluated for response who experienced CR or PR.

Toxicity was graded according to the Common Terminology Criteria for Adverse Events (CTCAE) version 3.0. In cases of grade 4 thrombocytopenia,

doses of methotrexate, ifosfamide, and etoposide were reduced to two thirds of their previous levels in the second course. L-asparaginase was discontinued if it induced grades 3 or 4 allergic reactions/hypersensitivity, pancreatitis, or hypotension. If L-asparaginase induced grades 1 or 2 allergic reactions/hypersensitivity, the dose of L-asparaginase was reduced by half. In this case, the use of prednisone at a dose of 1 mg/kg/d was permitted. L-asparaginase was stopped if grade 4 thrombocytopenia or grade 3 nonhematologic toxicity was observed. In the cases for which the first course of L-asparaginase was discontinued, L-asparaginase was readministered if the patient recovered from grade 4 thrombocytopenia or grade 3 nonhematologic toxicity. If the concentration of methotrexate exceeded 1×10^{-7} mol/L 72 hours after the administration during the first course, the dose of methotrexate in the second course was reduced to two thirds.

Statistical Analysis

The primary end point was an ORR after two courses of SMILE chemotherapy. The secondary end points were CR rate after two courses of SMILE chemotherapy, 1-year overall survival (OS), response of the subgroup, or toxicity. The expected ORR was estimated to be 60%, and the threshold ORR was estimated to be 35%, on the basis of our previous observations.[6,19] With a statistical power of 80% and a one-sided, type I error of 5%, the number of eligible patients required for this study was calculated to be 25 using a binomial analysis method. The projected sample size was 28 patients, with an accrual of 3 years and the expectation that 10% of patients would be deemed ineligible.

OS was defined as the time from registration until death from any cause or until the date of the last follow-up for the patients who survived. Survival estimates were calculated using the Kaplan-Meier method, and the hazard ratio (HR) was estimated using a Cox regression. All analyses were performed using STATA SE 10 software (STATA, College Station, TX).

RESULTS

Patient Characteristics

As a result of an excellent accrual, the study protocol was revised to increase the statistical power from 80% to 90% in March 2009. The projected number of patients for this study was increased from 28 to 38. Ultimately, 39 patients were enrolled from 19 institutions between July 2007 and October 2009. Histologic diagnosis of all patients except one was confirmed as ENKL by the Central Pathology Review Board. The single patient who was excluded from further analyses was judged to have CD56-positive rhabdomyosarcoma by the Central Pathology Review Board.

The baseline characteristics of 38 eligible patients are listed in Table 2. The median age was 47 years (range, 16 to 67 years), and the male:female ratio was 21:17. Twenty patients (53%) had newly diagnosed stage IV disease, 14 were in first relapse, and four were in primary refractory state. Two patients were treated with radiation alone as the initial therapy. Among the 16 patients who received chemotherapy as their first-line therapy, five patients were treated with anthracycline-containing chemotherapies, and 13 patients were treated with platinum-based regimens. Two patients were treated with chemotherapy containing both anthracycline and platinum.

Table 2. Baseline Patient Characteristics (N = 38)

Characteristic	No. of Patients	%
Age, years		
Median	47	
Range	16 to 67	
Sex		
Male	21	55
Female	17	45
Site(s) of involvement at diagnosis		
Upper aerodigestive tract	35	92
Extra-upper aerodigestive tract only	3	8
Disease state		
Newly diagnosed stage IV	20	53
First relapse	14	37
Refractory to the first-line treatment	4	11
Stage at enrollment		
IE or IIE	11	29
IIIE or IV	27	71
"B" symptoms present	18	47
Elevated serum LDH	16	42
Performance status		
0	21	55
1	12	32
2	5	13
Prior treatment		
None	20	53
Radiotherapy alone	2	5
Chemotherapy alone	3	8
Concurrent chemoradiotherapy	9	24
RT-DeVIC	6	
CCRT-VIPD or VIDL	2	
RT-CHOP	1	
Other combined modality therapies	4	11

Abbreviations: CCRT, concurrent chemoradiotherapy; DeVIC, dexamethasone, etoposide, ifosfamide, and carboplatin; LDH, lactate dehydrogenase; VIDL, etoposide, ifosfamide, dexamethasone, and L-asparaginase; VIPD, etoposide, ifosfamide, cisplatin, and dexamethasone.

Treatment

Twenty-eight patients (74%) completed the planned treatment. In two patients, the treatment was discontinued on day 4 because of methotrexate-associated encephalopathy and intestinal perforation owing to rapid tumor lysis. L-asparaginase was discontinued in four patients due to adverse events (AEs), including two patients with allergy to L-asparaginase (both in the second course), one patient with pancreatitis (grade 2, in the first course), and one patient with liver function derangement (in the first course). In two of these four patients, L-asparaginase was readministered at a 50% dose reduction. One allergic patient received simultaneously prednisolone 1 mg/kg. In another four patients, L-asparaginase was also stopped per protocol, owing to AEs of preceding agents (methotrexate, ifosfamide, and etoposide), including two patients with infections and two patients with thrombocytopenia. The relative dose-intensity of L-asparaginase in the first course of SMILE was 81%. Two of these eight patients who had L-asparaginase discontinued achieved CR. The relative dose-intensity of CR patients was 92%.

Additional courses of SMILE were given for 21 patients (one course, 10 patients; two courses, three patients; three courses, two patients; four courses, six patients). The median number of courses of SMILE administered was three (range, one to six courses). Treatment of the 28 patients who completed two courses of SMILE were as follows: chemotherapy only (n = 7), autologous HSCT (n = 4), or allogeneic HSCT (n = 17; myeloablative, n = 15, nonmyeloablative, n = 2). No difficulties in mobilizing peripheral blood HSC were encountered in the four patients who received autologous HSCT. Among the seven patients who did not complete the protocol treatment, two of them received no additional treatment and died as a

Table 3. Incidence and Maximum Severity of Adverse Events (N = 38)

Adverse Event	Grade 3 No.	Grade 3 %	Grade 4 No.	Grade 4 %
Hematologic				
Leukopenia	9	24	29	76
Neutropenia	3	8	35	92
Anemia	18	47	1	3
Thrombocytopenia	9	24	15	40
Nonhematologic				
Hypofibrinogenemia	4	11	0	0
APTT elongation	4	11	0	0
Hypoalbuminemia	6	16	0	0
Hyperbilirubinemia	3	8	1	3
AST elevation	12	32	0	0
ALT elevation	10	26	2	6
Creatinine	2	5	0	0
Hyponatremia	11	29	1*	3
Hyperglycemia	7	18	0	0
Amylase	6	16	1*	3
Appetite loss	8	21	1*	3
Diarrhea	4	11	0	0
Nausea	5	13	0	0
Mucositis	5	13	0	0
Vomiting	2	5	0	0
Infection	17	45	6†	16
Somnolence	1	3	2	5
Encephalopathy	0	0	1	3

NOTE. Grade 3 hypernatremia, allergic reaction, fever, and dehydration were observed in one patient each.
Abbreviation: APTT, activated partial thromboplastin time.
*Related to grade 2 pancreatitis in one patient.
†Including the two patients who died as a result of infection (two treatment-related deaths).

result of disease. Three patients were treated with other chemotherapy, and two of them underwent allogeneic HSCT without response.

Toxicity

Table 3 lists all grade 3 or 4 AEs that occurred in the 38 eligible patients who were enrolled onto this trial. After the death of initial two patients from grade 5 infections (patients 1 and 2; see Appendix, online only), the protocol was revised to include a careful assessment of infection and the incorporation of a lymphocyte count of $\geq 500/\mu L$ into the eligibility criteria. There were no subsequent treatment-related deaths.

Grade 4 neutropenia was common (92%). The nonhematologic grade 4 toxicities included infection (n = 6), hyperbilirubinemia (n = 1), ALT elevation (n = 2), and encephalopathy (n = 1); two patients experienced grade 4 somnolence, which was complicated by a grade 3 infection in one patient and by grade 4 encephalopathy in the other patient. One patient experienced grade 2 pancreatitis and had complications from grade 4 hyponatremia, hyperamylasemia, and appetite loss. The most common grade 3 nonhematologic AE was infection (45%). Allergic reactions due to L-asparaginase of any grade were observed in five patients (three with grade 1, one with grade 2, and one with grade 3). The toxic profiles according to disease status at the time of study entry (newly diagnosed/relapsed/refractory) are shown in Appendix Table A1 (online only). The grade 4 hematologic toxicity rates of newly diagnosed and relapsed patients were 95% and 93%, respectively. The grade 4 nonhematologic toxicity rates of newly diagnosed and relapsed patients were 35% and 14%, respectively. None of these differences were statistically significant ($P = .99$ and $P = .25$). No clinical predictors of toxicity were found. Only hyponatremia was associated with newly diagnosed and refractory diseases.

Table 4. Response After Two Cycles of SMILE Chemotherapy (N = 38)

Response	All Patients (N = 38) No.	All Patients (N = 38) %	Newly Diagnosed Stage IV (n = 20) No.	Newly Diagnosed Stage IV (n = 20) %	First Relapse (n = 14) No.	First Relapse (n = 14) %	Refractory to the First-Line Therapy (n = 4) No.	Refractory to the First-Line Therapy (n = 4) %
CR	17	45	8	40	9	64	0	0
PR	13	34	8	40	4	29	1	25
NR	1	3	1	5	0	0	0	0
PD	4	10	1	5	1	7	2	50
ED	3	8	2	10	0	0	1	25

Abbreviations: CR, complete response; ED, early death; NR, no response; PD, progressive disease; PR, partial response; SMILE, steroid (dexamethasone), methotrexate, ifosfamide, L-asparaginase, and etoposide.

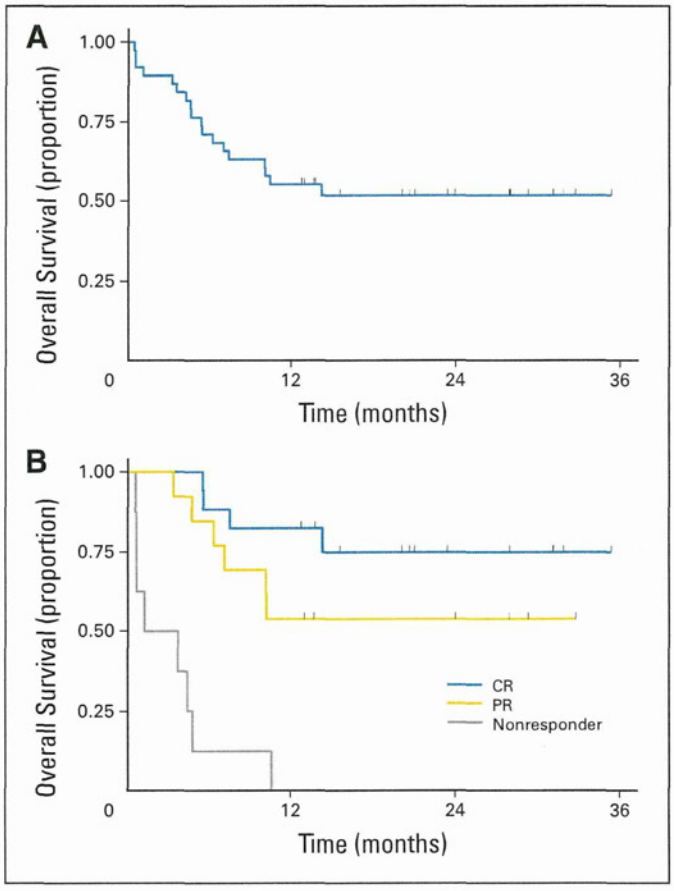

Fig 1. Kaplan-Meier estimates of overall survival (OS) of patients treated with steroid (dexamethasone), methotrexate, ifosfamide, L-asparaginase, and etoposide chemotherapy. (A) The 1-year OS of 38 patients was 55% (95% CI, 38% to 69%). The median follow-up of survivors was 24 months (range, 13 to 35 months). (B) The 1-year OS was 82% (95% CI, 55% to 94%) for patients who attained complete response (CR) and 54% (95% CI, 25% to 76%) for those who attained partial response (PR).

Efficacy and Survival

Among the 38 eligible patients, the response was CR in 17 patients (45%), PR in 13 patients, no response in one patient, progressive disease in four patients, and early death in three patients (Table 4). The ORR was 79% (90% CI, 65% to 89%). There were no differences in either the ORR or CR rate between patients with newly diagnosed stage IV disease and those with first-relapse disease. With respect to progressive disease in four patients, one occurred during the first course of SMILE, one after the first course, and two after the completion of two courses.

The median follow-up time of the living patients was 24 months, with a range of 13 to 35 months. The OS rate at 1 year, which was one of the secondary end points, was 55% (95% CI, 38% to 69%; Fig 1A). The progression-free survival (PFS) at 1 year was 53% (95% CI, 36% to 67%). The patients who attained response with SMILE chemotherapy had a higher OS (Fig 1B). The OS and PFS by the disease state at entry are shown in Figure 2A and 2B. Patients with relapsed disease showed better 1-year OS (79%) and PFS (71%) as compared with patients with refractory disease (P = .04 and .05, respectively). The survival curves of patients (excluding early deaths; n = 35) according to the type of poststudy therapy (autologous/allogeneic HSCT/chemotherapy) are shown in Figures 2C and 2D. Patients who received autologous HSCT seemed to show better OS and PFS, but the difference was not statistically significant. Univariate analysis for OS showed that presence of B symptoms (HR, 3.1, P = .01), performance status of 1 or 2 (HR, 3.1, P = .002), elevated serum lactate dehydrogenase (HR, 6.1, P = .001), and hemoglobin of less than 12 g/dL (HR, 3.9, P = .007) were significant prognostic factors.

DISCUSSION

Our results indicate that SMILE chemotherapy is effective for the treatment of newly diagnosed stage IV, relapsed, or refractory ENKL. The ORR after two cycles of SMILE (79%; 90% CI, 65% to 89%) clearly exceeded the threshold ORR (35%).[20] The 1-year OS rate (55%) was much improved compared with the previous treatment strategy.

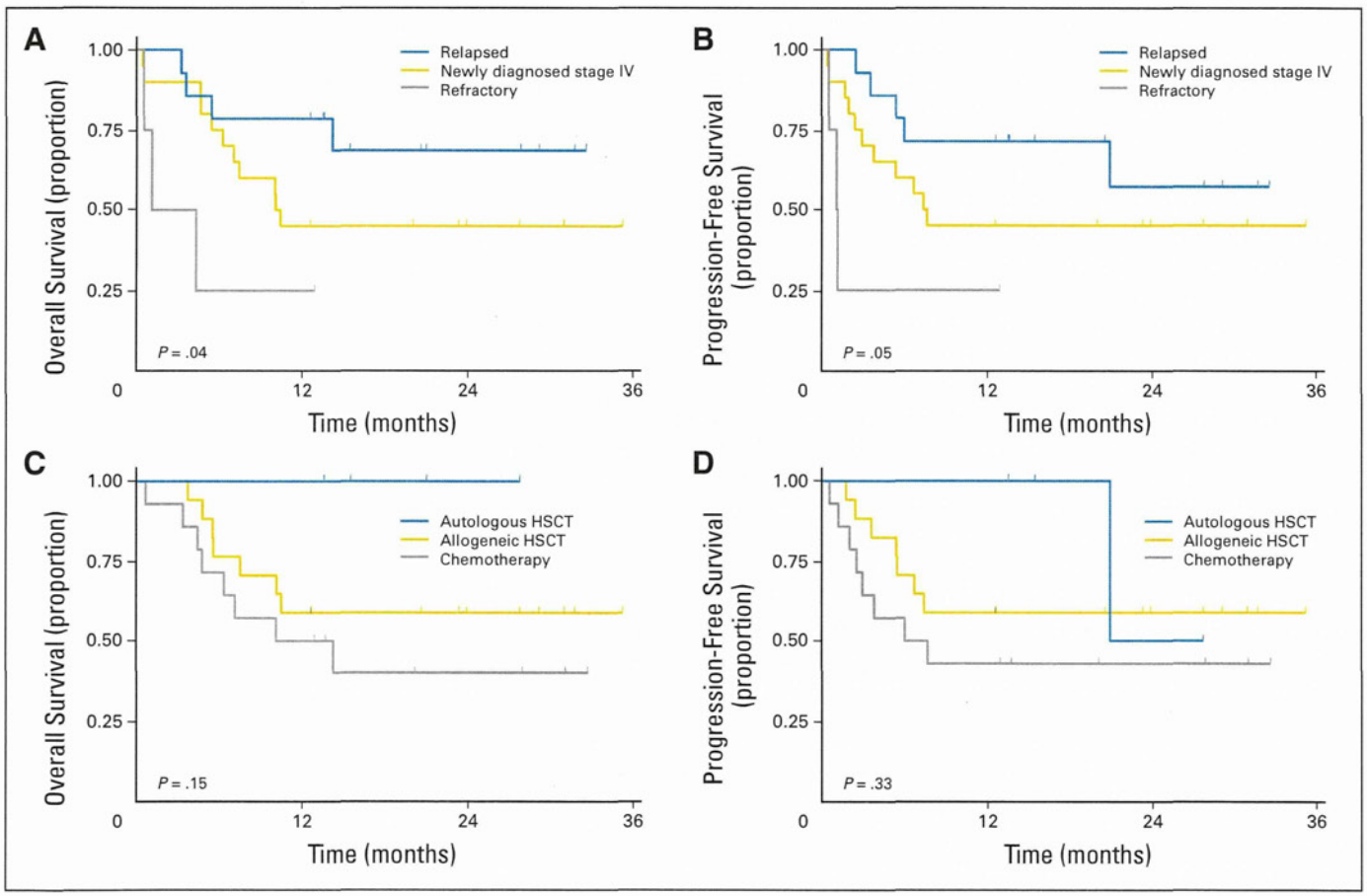

Fig 2. Kaplan-Meier estimates of overall survival (OS) and progression-free survival (PFS) of patients by the subgroup analysis. (A) OS of patients by the disease state at entry. The 1-year OS was 45% (95% CI, 23% to 65%) for patients with newly diagnosed stage IV disease, 79% (95% CI, 47% to 93%) for patients with relapsed disease, and 25% (95% CI, 1% to 67%) for patients with refractory disease. The difference was statistically significant (P = .04). (B) PFS of patients by the disease state at entry. The 1-year PFS was 45% (95% CI, 23% to 65%) for patients with newly diagnosed stage IV disease, 71% (95% CI, 41% to 88%) for patients with relapsed disease, and 25% (95% CI, 1% to 67%) for patients with refractory disease. The difference was statistically significant (P = .05). (C) OS of patients excluding early death (n = 35) by type of poststudy therapy. The 1-year OS was 100% for patients who received autologous hematopoietic stem-cell transplantation (HSCT), 59% (95% CI, 36% to 78%) for patients who received allogeneic HSCT, and 41% (95% CI, 19% to 63%) for patients treated with chemotherapy only. The difference was not statistically significant (P = .15). (D) PFS of patients excluding early death by type of poststudy therapy. The 1-year PFS was 100% for patients who received autologous HSCT, 59% (95% CI, 36% to 78%) for patients who received allogeneic HSCT, and 35% (95% CI, 14% to 57%) for patients treated with chemotherapy only. The difference was not statistically significant (P = .33).

